





Advancing geological and structural understanding of the Atuba Complex: a study in the Curitiba Terrane of the Southern Ribeira Belt, Southern Brazil

Michelangelo Tissi Baldin^{1*} , Eduardo Salamuni² , Leonardo Evangelista Lagoeiro² , Emerson Sanches² 

Abstract

The Atuba Complex occurs in the eastern region of Paraná State, located in the Southern Ribeira Belt. It is comprised of the Curitiba Terrane, northward of the Luís Alves Terrane, and southward of the Apiaí Terrane. This research was carried out by means of detailed petrography, microtectonics, and brittle and ductile structural analysis. The Atuba Complex is composed of migmatites, felsic granulites, granitoids, quartzites, phyllonites, schists, amphibolites, and cataclasites. The lithotypes are cut by diabase or gabbro dikes, lamprophyre dikes, pseudotachylites, and quartz, epidote, carbonate, or chlorite veins. The migmatites are characterized by two migmatization phases, the first composed of tonalitic leucosomes and the second formed by granitic leucosomes. The stromatic and mylonitized migmatites suggest dislocation creep mechanisms and dynamic recrystallization processes, mainly in quartz and feldspars. During the initial phase, melting reactions took place through dehydration, while in the subsequent phase, melting was facilitated by the presence of water-fluxed. The Atuba Complex comprises two foliations, S_{n-1} (D_{n-1} phase) and S_n (D_n phase). The S_{n-1} surface (compositional banding) presents a ductile and anastomosed aspect with an N45W/S5NE attitude, whereas the S_n mylonitic foliation is defined by the presence of mineral flattening or stretching and by the orientation of amphibole and biotite shapes, with a maximum plane of N45E/85NW. The observed faults and fractures strike in the NE-SW and NW-SE main directions. The paleostress study provided the recognition of a NE-SW sigma 1 associated with a NW-SE-striking sigma 3 for the left-lateral strike-slip faults and an E-W compressive SHMAX and an N-S distensive SHMIN for the right-lateral strike-slip faults.

KEYWORDS: Atuba Complex; microtectonics; structural analysis; migmatites.

INTRODUCTION

Since the beginnings of geology up to the most recent advances, migmatites have challenged scientists with their complex origin and evolution. They are composed of bands of leucosomes (light areas rich in minerals like quartz and feldspar) and melanosomes (dark areas rich in mafic minerals such as biotite and amphibole), found in various parts of the world, especially in areas with intricate tectonic history and significant metamorphic activity (Sawyer 2008). Migmatite complexes are fascinating and important because they provide insights into heterogeneous geological processes, including partial melting, fluid migration, metamorphism, and the tectonic evolution of deep crustal regions. These complexes are found in various parts of the world; some notable examples include Mount Stafford in Australia (White *et al.* 2003),

Thor-Odin Dome in Canada (Vanderhaeghe and Teyssier 2001), Sand River Gneisses in South Africa (Sawyer 2008), Port Navalo area in France (Marchildon and Brown 2003), and the Colorado Front Range in the United States (Olsen and Grant 1991).

Structures found in migmatite complexes can be extremely varied and interesting, offering insights into the region's history. Some of the most common structures include compositional banding, folds, shear zones, veins, and xenoliths (Ashworth 1985). The study of these structures is essential for understanding the geological processes that have affected the Earth's crust over time and for interpreting the tectonic evolution of the areas where migmatite complexes are found, potentially indicating continental collision events or lateral movements (Sawyer 2008, Sawyer and Brown 2008). However, for a comprehensive study of these structures, it is crucial to establish an appropriate classification of migmatites, which can be achieved based on reference works by prominent researchers such as Mehnert (1968), Brown (1973, 1979, 1994, 1998), Ashworth (1985), and Sawyer (1998, 1999, 2001, 2008).

The present work aims to address research questions related to the various structures found in the migmatites of the Atuba Complex (Curitiba Terrane), essentially considering the contributions of Mehnert (1968) and Sawyer (2008). In this context, the main characteristics defining migmatites will be discussed, as well as their importance for understanding the

¹Universidade de São Paulo, Mineralogia e Geotectônica, Instituto de Geociências – São Paulo (SP), Brazil. E-mail: miche_georock@yahoo.com.br

²Universidade Federal do Paraná (UFPR), Setor de Ciências da Terra, Departamento de Geologia – Curitiba (PR), Brazil. E-mails: salamuni@ufpr.br, leonardo.lagoeiro@ufpr.br, esanches.emerson@gmail.com

*Corresponding author.



geological processes involved in the formation of these metamorphic rocks. Additionally, detailed studies on migmatites using advanced mapping, petrography, and structural geology techniques are essential to expand our understanding of the Southern Ribeira Belt and the Curitiba Terrane.

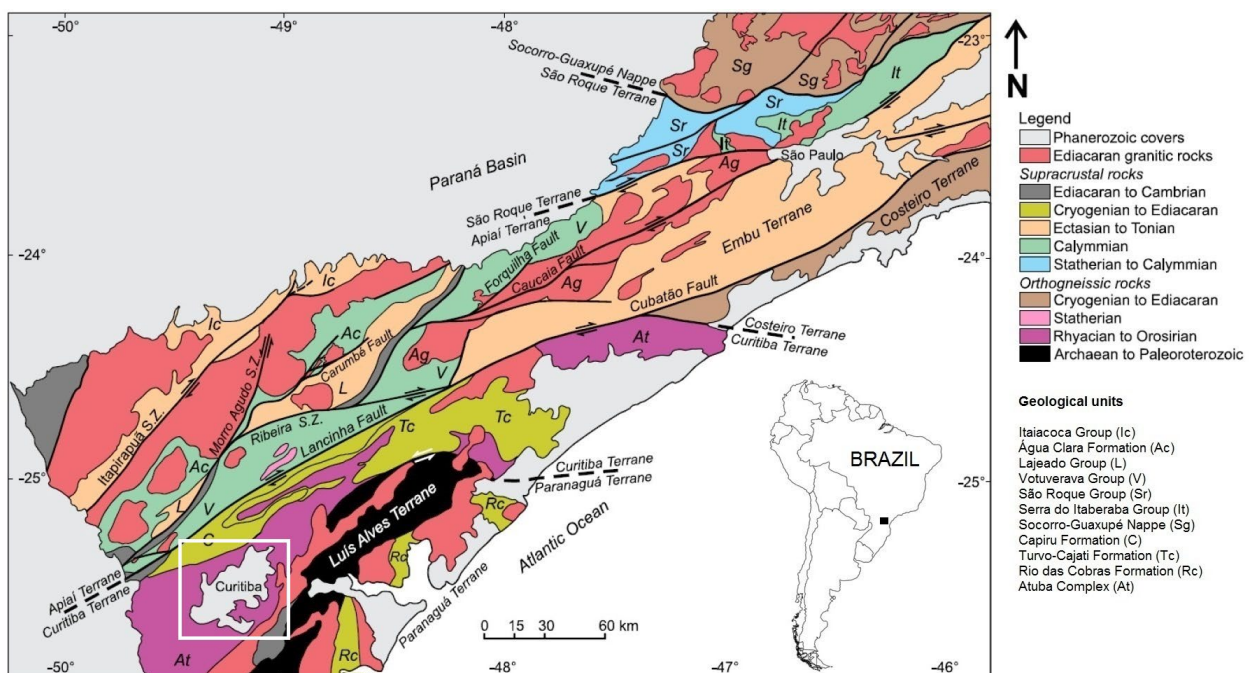
The Atuba Complex is in the eastern region of Paraná State and the southwestern portion of São Paulo State (Faleiros 2008, Faleiros *et al.* 2016, Fig. 1). The study area is in eastern Paraná State, in Curitiba city and surrounding regions, covering the municipalities of Colombo, Campo Largo, Quitandinha, Balsa Nova, and São José dos Pinhais. It covers approximately the western longitudes 49°00' and 49°40' and the southern latitudes 25°10' and 25°50'. All the outcrops were selected by using road and geological maps, due to the structural interest, access, and representativeness of the Atuba Complex.

The Atuba Complex is a prominent and intricate geological unit that has drawn significant interest among geologists due to its unique characteristics and geological history. It comprises a variety of rocks, including gneisses, migmatites, granites, amphibolites, and schists, among others (Siga Junior *et al.* 1995, Silva *et al.* 1998). These rocks have undergone extensive metamorphism and deformation over billions of years, making the complex a crucial site for studying Earth's crustal processes. One of the most significant features of the Atuba Complex is the presence of migmatites. Their presence in the Atuba Complex indicates a history of high-grade metamorphism and partial melting events, providing valuable information about the geological evolution of the region (Siga Junior 1995). Researchers have conducted studies in the Atuba Complex (Siga Junior *et al.* 1995, Sato *et al.* 2003, 2009, Faleiros *et al.* 2011, 2016, Passarelli *et al.* 2018) to understand its geological history, structural features, geochemistry, and geochronology, along with petrography. Despite advancements in understanding

the Atuba Complex, there are still gaps in knowledge and unanswered questions. This includes the sequence of geological events, the tectonic processes that shaped the region, and the nature of geological boundaries within the complex.

Over the years, studies have revealed significant progress in our understanding of these geological systems; however, knowledge gaps still require deeper analysis. Despite researchers' efforts, there remain unanswered questions about migmatites and the interplay between petrographic and structural processes. The importance of this study lies in the scarcity of detailed information about the geological characteristics of the Atuba Complex and its relationship with the geology of the Curitiba Terrane and the Southern Ribeira Belt. So far, research in this region has been limited and fragmented, hindering a complete understanding of its geological evolution and the tectonic processes that have acted over time.

In this article, we aim to explore these gaps, bringing new perspectives to the understanding of migmatites and migmatite complexes in general, with a special focus on the Atuba Complex. We present an integrated analysis of petrographic, structural, deformational, and microstructural aspects, along with ductile and brittle analyses, highlighting the relevance of this study for the geological community and the importance of the addressed problem. By identifying and correlating different lithologies, metamorphic contexts, and structures present in the rocks, we can more accurately reconstruct the evolutionary history of the region. Furthermore, our detailed analyses allowed for the identification of fundamental tectonic processes that contributed to the formation of these rocks. Through a comprehensive investigation, this research aims to shed light on the broader understanding of tectonic processes in the region, providing a solid foundation for future investigations in this fascinating area of geosciences.



Source: modified from Forero-ortega *et al.* (2020).

Figure 1. Simplified geological map of the Southern Ribeira Belt. The work area is represented by the white rectangle on the map.

REGIONAL GEOLOGY

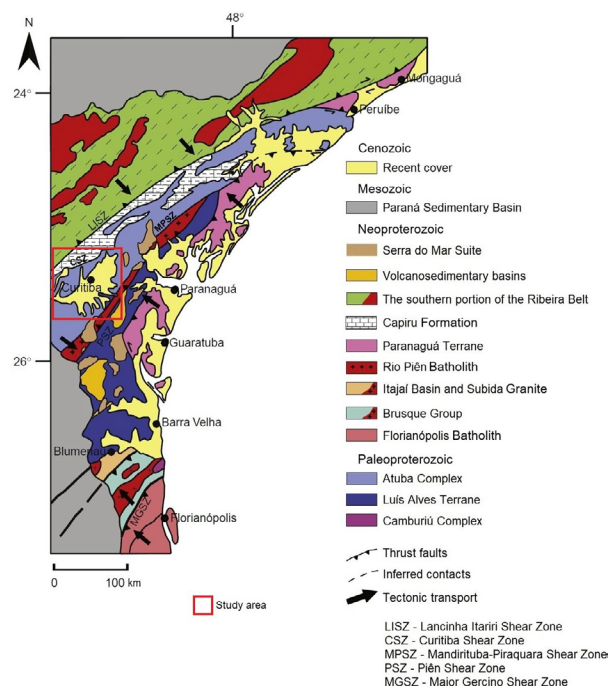
The Mantiqueira Province is in eastern Brazil and extends in the NNE direction for 3,000 km (Heilbron *et al.* 2004, 2008). It is formed by crustal fragments of different ages and evolutions that contributed to Western Gondwana's consolidation (Brito Neves and Cordani 1991). It is divided into the Dom Feliciano (south), Ribeira (central), and Araçuaí (north) belts (Heilbron *et al.* 2004).

The Ribeira Belt is NE-SW-oriented and is associated with the amalgamation, deformation, and metamorphism of Western Gondwana during the Neoproterozoic (Campanha and Sadowski 1999, Campanha and Brito Neves 2004). It presents counterparts in the Kaoko and Congo belts in Western Africa (Almeida *et al.* 1973) and appears as a product of the collision between the São Francisco, Congo, and Paranapanema cratons. The Southern Ribeira Belt (Fig. 1) is composed of tectonostratigraphic terranes that were bounded by strike-slip faults or shear zones (Heilbron *et al.* 2004, Faleiros *et al.* 2011). It comprises the Apiaí, Curitiba, Luís Alves, and Paranaguá terranes (Faleiros 2008).

The Curitiba Terrane is a narrow NE-SW belt, extending 50–60 km in length. It is composed of migmatitic orthogneisses and granitic intrusions of the Atuba Complex (Siga Junior *et al.* 1995). Shallow continental shelf metasedimentary rocks from the Turvo-Cajati Formation (Faleiros 2008, Faleiros *et al.* 2011, 2016) cover the northern portion of the Atuba Complex. They are formed by dolomitic marbles, quartzites, and phyllites (Faleiros *et al.* 2011). The Turvo-Cajati Formation is composed of rocks with maximum deposition ages of around 650–630 Ma (Faleiros *et al.* 2016) and metamorphism of 590–585 Ma (Faleiros *et al.* 2011, 2016). The formation consists of metamorphism in conditions ranging from lower greenschist facies to granulite facies (Faleiros 2008). Four metamorphic zones are recognized for the Turvo-Cajati Formation: biotite, garnet, staurolite, and sillimanite zones. Available petrological and geochronological data suggest that the formation comprises a paired metamorphic belt of low and high pressure, associated with an important suture zone in the south of the Ribeira Belt (Ricardo *et al.* 2020).

The Capiru Formation (Bigarella and Salamuni 1956) or Capiru Group (Santos *et al.* 2021) is a low-grade metasedimentary unit that outcrops in the Curitiba Terrain and records passive to active stages of the continental margin. It was deposited on the northern margin of the Curitiba Terrane, with an “exotic” Mesoproterozoic contribution (Santos *et al.* 2022). The lithostratigraphic units of the Capiru Group reflect depositional and tectonic events, which involved passive deposition of the continental margin; compressive episodes during the Late Neoproterozoic; and extensional tectonic processes, which culminated in the opening of the Proto-Atlantic Ocean (Santos *et al.* 2021).

The area under investigation is located in the southern portion of Mantiqueira Province and partially covers the southern portion of the Ribeira Belt in eastern Paraná State (Fig. 2). The Atuba Complex covers an extensive portion of eastern Paraná and is bounded to the south by the Rio Piên Suite deformed granites. It is bounded to the north by the metavolcanosedimentary



Source: modified from Basei *et al.* (2009).

Figure 2. Simplified geological and tectonic map of southern Brazil.

rocks of the Apiaí Terrane and to the southeast by the gneissic-granulite rocks of the Luís Alves Terrane (Siga Junior *et al.* 1995, Faleiros *et al.* 2016). The eastern portion is dominated by an igneous complex named Paranaguá Terrane (Cury 2009). The northern and northwestern boundaries are marked by the Lancinha Shear Zone, which represents a suture zone that separates the Atuba Complex from the terranes located to the north (Basei *et al.* 1992, 2008). In the southern portion, there are the Mandirituba-Piraquara and Piên-Tijucas shear zones.

The Atuba Complex is essentially composed of banded orthogneisses and migmatites with stromatic structures and compositional banding, where melanosomes and leucosomes of tonalitic-granodioritic composition alternate (Siga Junior *et al.* 1995, Faleiros *et al.* 2011, 2016). Leucosomes are fine-to coarse-granulated. Quartzite, quartz schists, mica schists, granulites, diabase, gabbro, and microdiorites dikes also occur (Fuck *et al.* 1967). The gneisses are leucocratic, with mesocratic and medium-grained terms. The texture is granonematoblastic, granolepidoblastic, and granoblastic (Siga Junior 1995, Siga Junior *et al.* 1995). Rare-earth element patterns are strongly fractionated and can present positive Eu anomalies (Siga Junior *et al.* 1995).

During the Paleoproterozoic, intense migmatization occurred between 1900 Ma and 2200 Ma, without much activity in the Mesoproterozoic (Sato *et al.* 2003). In the Brasiliano-Panafrican event, the tectonothermal reworking was dated at 633 Ma and 645 Ma by U-Pb SHRIMP and EV-TIMS in zircon crystals (Passarelli 2001, Sato *et al.* 2003). The main geochronological data available for the Atuba Complex can be seen in Table 1. Faleiros (2008) showed geothermobarometric estimates and P-T path quantifications for the Atuba Complex, with practically isobaric cooling from 750°C for Paleoproterozoic migmatization to a re-equilibrium around 650–700°C and 6–7 kbar in the Neoproterozoic.

Table 1. Available isotopic data for the Atuba Complex.

Methods/materials	Localizations	Lithotypes	Ages	References
First phase of migmatization				
U–Pb zircon (ID-TIMS)	Near Curitiba-PR	Granulitic gneiss	2095 ± 5 Ma	Siga Junior <i>et al.</i> (1995)
U–Pb zircon (ID-TIMS)	Mandirituba-PR	Amphibole-gneiss	2138 ± 6 Ma	Siga Junior <i>et al.</i> (1995)
U–Pb zircon (ID-TIMS)	Serra do Azeite-SP	Banded granitic gneisses	2148 ± 37 Ma	Vasconcelos <i>et al.</i> (1999)
Rb–Sr WR	NE of Curitiba	Granulitic gneiss	2116 ± 95 Ma	Siga Junior <i>et al.</i> (1995)
Rb–Sr WR	NE of Curitiba	Biotite-amphibole-gneiss migmatitic	2220 ± 26 Ma	Siga Junior <i>et al.</i> (1995)
Rb–Sr WR	Mandirituba-PR	Amphibole migmatitic gneiss	2010 ± 60 Ma	Siga Junior <i>et al.</i> (1995)
Second phase of migmatization				
U–Pb zircon (SHRIMP)	Near Curitiba-PR	Banded granitic gneisses	600 Ma	Kaulfuss (2001)
U–Pb zircon (ID-TIMS)	Near Curitiba-PR	Banded granitic gneisses	560–570 Ma	Kaulfuss (2001)
Rb–Sr WR	Atuba Quarry	Biotite-amphibole-gneiss migmatitic	598 ± 48 Ma	Siga Junior <i>et al.</i> (1995)
Rb–Sr mineral	Quitandinha-PR	Biotite-amphibole-gneiss migmatitic	577 ± 17 Ma	Siga Junior <i>et al.</i> (1995)
Sm–Nd isochron	Mandirituba-PR	Amphibole migmatitic gneiss	585 ± 30 Ma	Siga Junior <i>et al.</i> (1995)
K–Ar bio	Serra do Azeite-SP	Orthogneiss	527 ± 26 Ma	Campagnoli (1996)
Ar–Ar bio	Núcleo Setuva-PR	Orthogneiss	588 ± 1 Ma	Siga Junior <i>et al.</i> (2007)
Ar–Ar hbl	Serra do Azeite-SP	Pegmatitic vein	577 ± 3 Ma	Machado <i>et al.</i> (2007)

zr: zircon; bio: biotite; hbl: hornblende; ID-TIMS: isotope dilution thermal ionization mass spectrometry; WR: whole rock; SHRIMP: sensitive high-resolution ion microprobe.

Basei *et al.* (1992) observed the presence of muscovite, biotite, chlorite, zoisite, epidote, and second-generation quartz recrystallization as indicative of schist-greenstone facies retrograde metamorphism, chlorite, and biotite zones.

MATERIALS AND METHODS

The work was developed through petrography, microtectonics, and ductile and brittle structural analyses. It was divided into geographic information system (GIS) generation, field campaigns, petrography and microtectonics, and structural analysis.

Geographic Information System

The database was organized from the geological results extracted from the Curitiba Sheet, 1:250,000 scale (Mineropar 2006a) and Ponta Grossa Sheet, 1:250,000 scale (Mineropar 2006b), in addition to satellite imagery obtained through the Google Earth Pro service. A geological map was produced with the main foliations' attitudes. The software used was ArcGIS v. 10.2.

Field campaigns

The work aimed to describe in detail outcrops located along federal and state highways and in at least 14 active and deactivated quarries corresponding to the Atuba Complex to obtain geological and structural data (ductile and brittle). The method used for the field survey included the collection of foliations, lineation, mineral stretching, axial plane, folds axis and limbs, fractures, faults, and fault striae. Rock samples were systematically collected and oriented for petrographic and microtectonic studies.

Petrography and microtectonics

Descriptions of representative lithotypes were based on color, mineralogy, grain size, texture, and structure. A total of 147 thin sections were made in the Laboratory of Petrographic Lamination (LAMIN) and the Laboratory of Mineral and Rock Analysis (LAMIR). Microscopic analysis was performed on transmitted light petrographic microscopes (Olympus BX60 and LEICA DM 2500 P) of the Laboratory of Microscopy (LAPEM). Photomicrographs were obtained with the aid of an Olympus PM20 imaging system coupled to the petrographic microscope at LAMIR. The Axio Vision software (version 4.8.2.0) was used for capturing photomicrographs.

Sampling was carried out with structural and lithological control. In oriented samples, thin sections were made perpendicular to the foliation (x-y plane) and parallel to the mineral lineation (x-axis) for petrographic and microtectonic characterization. The morphological characterization of the migmatites followed the suggestions of Mehnert (1968) and Sawyer (2008). Mylonitic rocks and cataclasites were defined based on Sibson (1977). The name abbreviations of the occurring minerals were indicated according to the proposal of Whitney and Evans (2010).

Structural analysis

The structural data (planar and linear attitudes) were sorted in an Excel sheet (Office®), where the point numbers, Universal Transverse Mercator (UTM) coordinates, geographic locations, structure descriptions, and attitudes were inserted. The data statistical treatment was done in the Stereo 32 and Geotec Stereo v. 1.2.0.0 software (Fronza *et al.* 2016), through the construction of structural stereograms (Schmidt–Lambert), roses, and

density diagrams, for a better understanding of the structural pattern. For the paleostress diagrams, the Wintensor v. 5.8.9 software (Delvaux and Sperner 2003) was used, employing the right dihedral method (RDM) of Angelier and Mechler (1977). The approach used to analyze paleostress considering the dextral or sinistral sense of movement of the analyzed strike-slip faults involved examining the characteristics of fault planes, such as their geometry, orientation, and dip, in addition to the examination of synthetic shear fractures, antithetic shear fractures, and the arrangement of neoformed minerals. During field analysis, it was also important to observe other movement indicators, such as slickensides, slickenlines, steps, and layer displacements. The determination of the kinematic parameters of the faults was based on the criteria established by Petit (1987) and Doblas (1998). The kinematic analysis of the faults was carried out based on 98 fault planes measured in the field, with 36 sinistral fault planes and 62 dextral fault planes. Only faults with identifiable kinematic indicators on their surfaces, such as slickensides and steps, were examined. The faults were divided into specific orientations due to the better applicability and ease of the Wintensor v. 5.8.9 software (Table 2).

RESULTS

Within the scope of this section, we seek to improve connectivity and clarity in the description of the various structures presented in this manuscript. Recognizing the fundamental importance of understanding the relationships between migmatite structures and more recent ductile and brittle structures, we aim to review and refine this approach, ensuring a more effective exposure to these geological interconnections.

To achieve this goal, we opted for a sequential and logical organization of the descriptions, starting with the migmatite structures and progressively advancing to the youngest brittle structures. This approach seeks to provide a natural progression for understanding geological relationships. By adopting these strategies, we believe that our review in this section will contribute substantially to the global understanding of the

complex interactions between the geological structures discussed in this manuscript.

Macroscopic features

In this section, we describe the main types of rocks observed in the Atuba Complex. Macroscopic rock descriptions have played a crucial role in the geology of the area, offering a comprehensive and fundamental view of the physical and structural characteristics of the rocks of the Atuba Complex. These visual and tactile observations were vital for directly identifying the lithologies of the study region.

Migmatitic unit

The comprehensive interpretation of migmatitic features throughout the entire Atuba Complex unit required a rigorous approach supported by consistent data and arguments. It began with a detailed mapping of the area, identifying the spatial distribution of these features. The use of geological maps (Mineropar 2006a, 2006b) can provide a more comprehensive and accurate view. Collecting representative samples of migmatite rocks from different locations within the Atuba Complex was crucial. These samples were subjected to petrographic and microstructural analyses to unequivocally confirm the presence of migmatites throughout the unit. The detailed description of microscopic characteristics, highlighting minerals indicative of migmatization, was fundamental, as was the identification of textures that suggest migmatite processes, such as banding, folds, veins, and foliation. Furthermore, it was crucial to investigate the regional geological context to understand the relationship of the Atuba Complex with other surrounding geological units, evaluating whether the migmatite features are associated with specific tectonic events and whether they are consistent with the regional geodynamic context. Comparison with previous geological studies in the region offered valuable insights and allowed the consistency of interpretations to be verified.

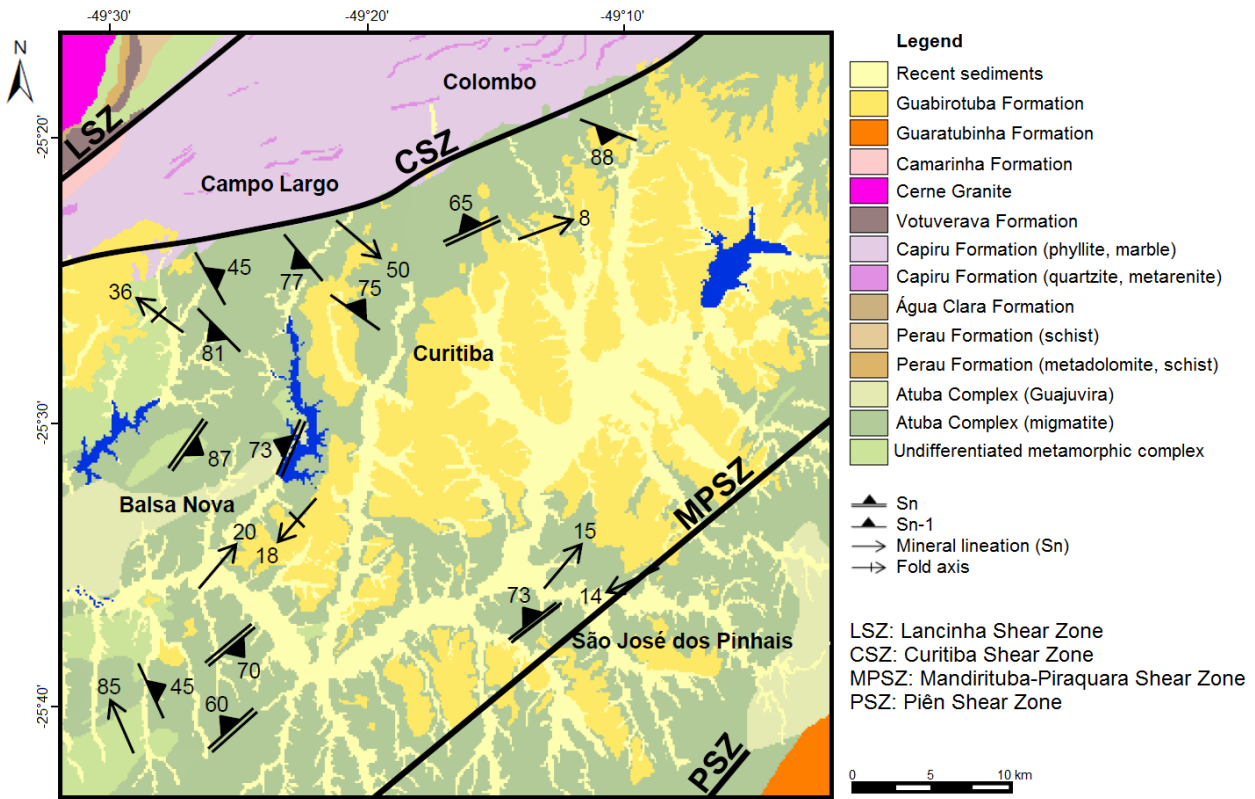
In the field, the distribution of the different rock facies, such as migmatites, granulites, amphibolites, schists, granitoids, quartzites, and phyllonites, reveals a rich geological tapestry. Migmatites generally occur near granitoids and granulites, with irregular or curved contacts. Amphibolites and quartzites are often interbedded with migmatites, while schists appear in varying associations. Phyllonites may cut across multiple facies or occur subparallel to the main migmatite foliation.

The migmatites (Fig. 3) observed can be patch, stromatic, schollen, with folded structures, dilation-structured, net-structured, protomylonitic to ultramylonitic, schlieric, venulated, and ophthalmic. All structures occur within a dekameter to kilometer distance.

Patch migmatites (Fig. 4A) show neosomes without segregation or separation between the leucosome and melanosome. They occur in punctual places, with oval or rounded and massive aspects. Locally, they are foliated, with mafic minerals' orientation. Patch migmatites are white, scattered throughout the migmatite, and consist mainly of plagioclase and quartz, with rare garnet, hornblende, and biotite crystals occupying the core and leucosome boundaries. The neosome

Table 2. Clar notation divisions for the fault directions identified in the study area.

Faults	Directions
F1	340–20
	160–200
F2	310–340
	130–160
F3	285–310
	105–130
F4	255–285
	75–105
F5	230–255
	50–75
F6	200–230
	20–50



Source: modified from Mineropar (2006a, 2006b).

Figure 3. Geological and structural map of the eastern Paraná State, showing the Atuba Complex and surroundings.

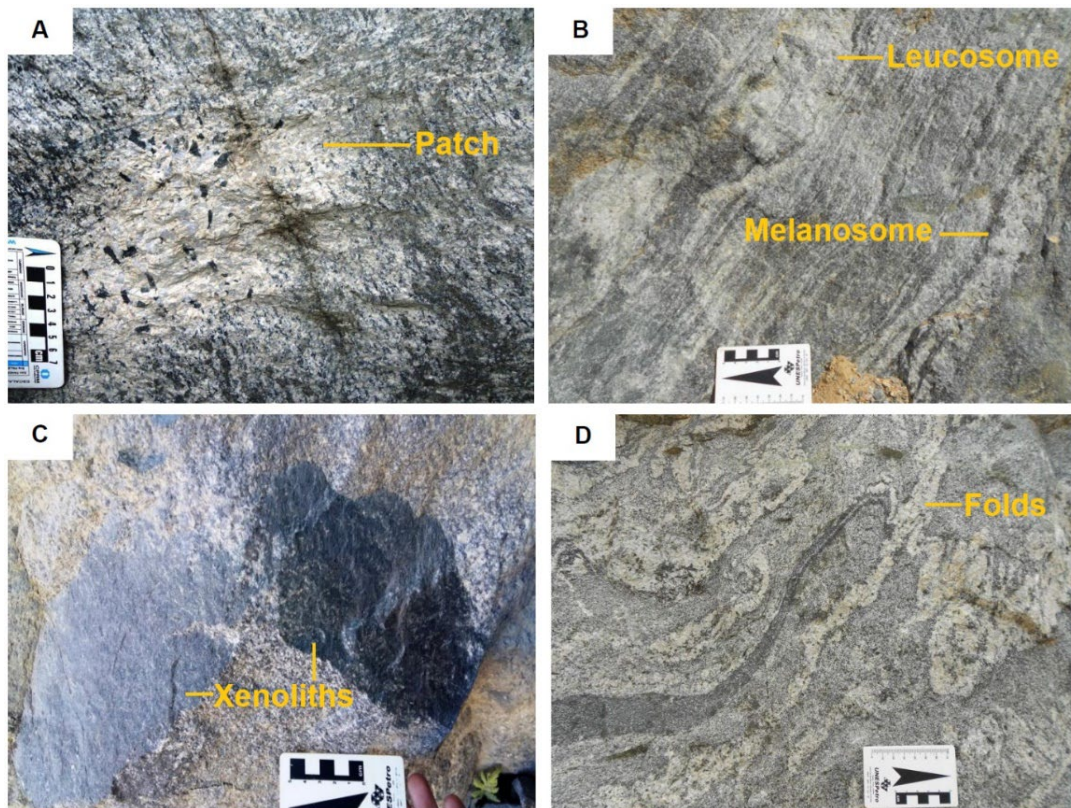


Figure 4. Migmatites from the Atuba Complex. (A) Patch-type migmatite is characterized by having distinct areas of leucosomes distributed in an irregular and unsystematic manner within the rock matrix. These areas form scattered “spots” or “patches” varying in size and shape. The resulting texture is generally granoblastic, defined by the equidimensional arrangement of nonoriented minerals. (B) Stromatic migmatite exhibits an organized structure, with alternating light bands (leucosomes) and dark bands (melanosomes). These bands are generally parallel or have slight foliation, and the distribution of leucosomes and melanosomes is more regular than in patch migmatites. (C) Schollen migmatite exhibits a texture characteristic of melanocratic enclaves surrounded by a lighter rock matrix. Enclaves can vary in size and shape, and their distribution is not uniform. (D) Migmatite with a folded structure exhibits folds of different scales, from small to large, that affect the entire rock. These folds can be apparent in both leucosomes and melanosomes, contributing to the structural complexity of the rock.

exhibits coarser graining than the rest of the rock and remains in situ. Some patches are elongated along the compositional banding direction.

The stromatic migmatites (Fig. 4B) are heterogeneous on a macroscopic to microscopic scale. They have an alternation of leucosome, melanosome, and residual mesocratic neosome. The leucosome has light-colored levels of quartz-feldspathic composition, and the melanosome has dark-colored levels, rich in ferromagnesian minerals. The millimetric to centimetric-thick white leucosome exhibits parallel orientation with the gneissic or compositional banding of the mesocratic neosome, maintaining lateral persistence. The pink leucosome presents a granulation that varies from fine to coarse, is occasionally pegmatitic, and conforms to the main foliation of the rock. It consists of potassium feldspar, quartz, and plagioclase. The granitic leucosomes cut through the white leucosomes (tonalitic) in the form of pockets and tabular or irregular veins. Contacts between leucosomes and melanosomes can vary in sharpness and complexity. In some areas, these contacts may be abrupt or irregular. In other regions, contact may be gradual. Melanosomes often exhibit a variety of shapes, from irregular lenses to elongated bands. Granoblastic textures can be observed in leucosomes, and in melanosomes, textures can vary from granoblastic to granonematoblastic, where minerals such as biotite and amphibole can appear oriented.

Schollen-type (raft) migmatites show a transition from stromatic metatexite to diatexite. The schollen or rafts-type migmatites (Fig. 4C) are found in gneissic or granitic matrix, medium- to coarse-grained. The xenoliths are angular or rounded and sometimes may rotate. They are metamorphic, thin- to medium-grained, rounded, or angular, dark gray, and composed of pyroxene, amphibole, and biotite. The xenoliths often exhibit boudinage and hydraulic fracturing. Internal domains may show leucosome bands with irregular contours or with tight folds that are truncated by the schollen boundaries. It rarely occurs with a narrow biotite-rich edge (selvedge). Occasionally, the major xenolith elongation is parallel to the stromatic metatexite S_n foliation.

Folded-structured migmatites (Fig. 4D) have a medium gray color, fine, medium, or coarse granulation, and are formed by quartz, feldspars, biotite, and amphiboles. They exhibit centimetric to metric folds, consisting of lighter leucocratic zones rich in felsic minerals and darker melanocratic zones rich in mafic minerals. Folded-structured migmatites may exhibit a slight thickening of the leucosome in the hinge region relative to the fold limbs. The leucosome is millimetric or centimetric, and sometimes the melanosome occurs as short, thin bands parallel or subparallel to the leucosome.

Migmatites with a dilation structure (Fig. 5A) can be lighter in color and vary in color, often exhibiting shades of white to pale gray. These migmatites often exhibit distinct patterns of leucocratic (light) and melanocratic (dark) zones. The clear zones are formed by felsic minerals such as quartz and feldspar. Dark zones contain mafic minerals such as biotite and hornblende. They are found at specific and restricted levels and appear as boudins.

The net-structured migmatites (Fig. 5B) have narrow, irregular leucosomes in two or more directions, surrounded by thin, dark gray melanosomes formed by biotite and hornblende. The leucosome injections are characterized by plagioclase, K-feldspar, and quartz and produce a polygonal pattern in the rock. They are 1–10 cm thick and asymmetrically distributed. There are mainly two trends of structures, one being subparallel and the other obliquely discordant ($30\text{--}45^\circ$) to the S_n foliation.

The migmatites with protomylonitic to ultramylonitic textures (Fig. 5C) are gray-colored and fine- to medium-grained. There are reductions in grain size and mineral stretching, with moderately rounded feldspar porphyroclasts and a matrix composed of quartz-feldspathic levels. They possess mylonitic texture, defined by the orientation of biotite and quartz. The foliation is characterized by parallel or anastomosed layers, often folded, marked by elongated minerals such as mica and quartz.

The schlieric-type migmatites (Fig. 5D) are dark gray in color and are formed mainly by micaceous minerals, consisting of millimeter- to centimeter-thick layers or bands in a straight or curved shape. They often exhibit flow foliation, defined by the parallel and lamellar disposition of the biotite, resulting from the alignment of the crystals. The structure is well developed, where biotite and amphibole trails (schlieren) occur in an oriented form. Locally, clusters of mafic minerals encompassed or fragmented by the leucosome are observed. Some schollen may be present.

The venulated-structured migmatites (Fig. 5E) are composed of quartz-feldspathic veins that cut the foliation or the compositional banding in different directions, with a massive or foliated aspect. They are characterized by intricate patterns of veins running through the rock. These patterns resemble a network of interconnected or branching veins, which can vary in thickness and shape.

The ophthalmic migmatites (Fig. 5F) are unequigranular, thin to thick, leucocratic to mesocratic, and have a granitic to granodioritic composition. The paragenesis consists of K-feldspar, quartz, and plagioclase, in addition to biotite and amphibole. The texture is porphyrogranoblastic to granonematoblastic, and the rock color is light gray or pinkish. In general, centimetric K-feldspar porphyroclasts stand out, preferentially oriented, with a lenticular (augen) and elongated aspect, being contoured by biotite crystals. They define the rock foliation, together with fine- to medium-grained amphibole crystals.

Felsic granulites

The granulites are medium- to coarse-grained and gray. They are mainly composed of feldspars, quartz, amphibole, pyroxene, and garnet. They have a granoblastic and crystalline texture. The foliation is banded or massive. The banding often displays characteristically oriented minerals, alternating dark and light bands. The granulites may be moderately altered by claying and oxidation, affecting the rock's color, texture, and mineral composition.

Atuba Complex-associated rocks

The rocks associated with the Atuba Complex are divided into amphibolites, schists, granitoids, quartzites, and phyllonites.

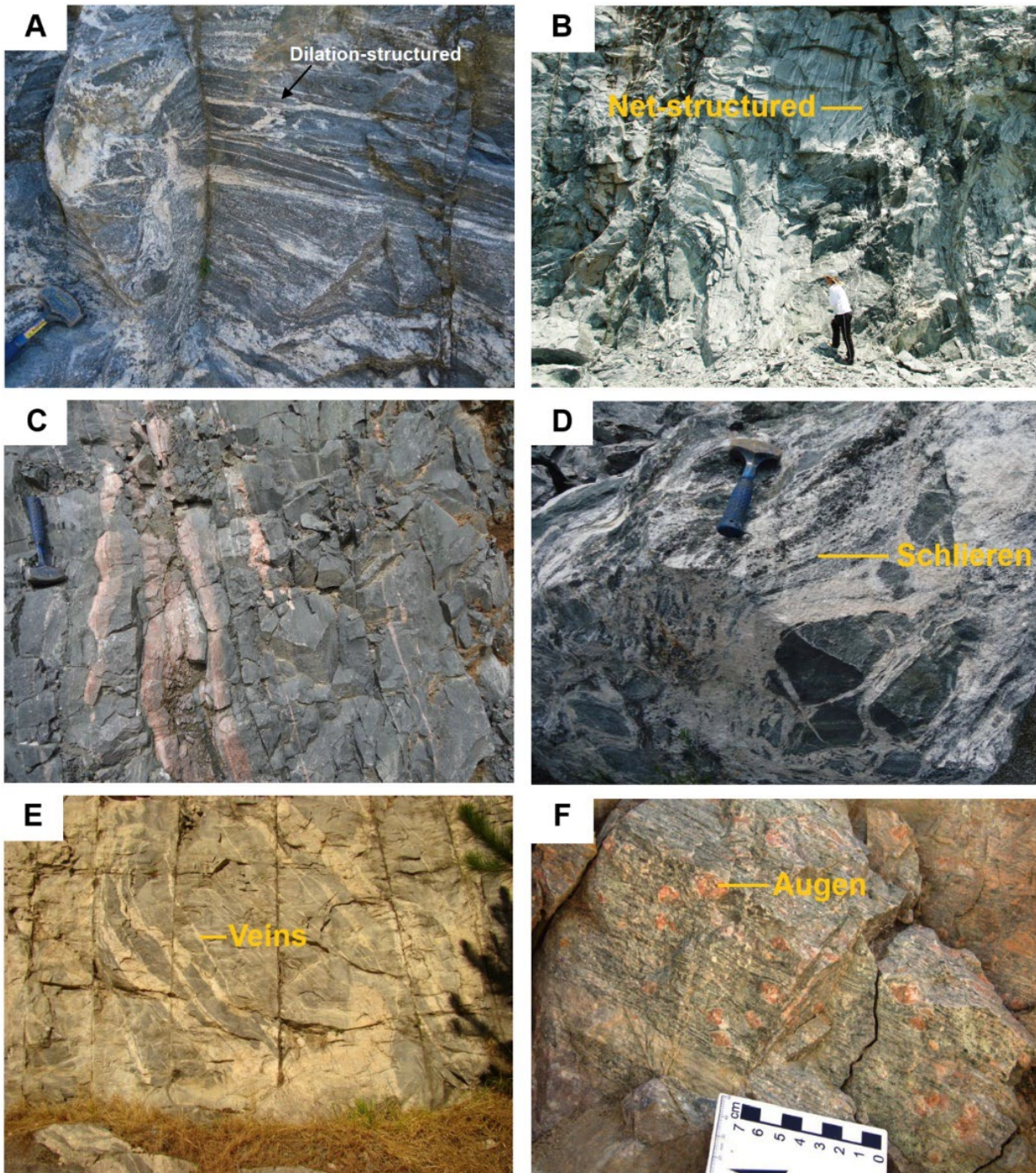


Figure 5. Migmatites from the Atuba Complex. (A) Dilation-structured migmatite. (B) Net-structured migmatite. (C) Ultramylonitic migmatite. (D) Schlieric migmatite. (E) Venulated migmatite. (F) Oftalmitic (augen) migmatite.

The amphibolites outcrop as lenses or elongate bodies, intercalated with stromatic migmatites. They are centimetric in thickness and commonly follow the main NE-SW-striking S_n foliation. They are dark gray, fine- to medium-grained, and can be massive or foliated. The mineralogy is dominated by amphibole and other associated minerals, such as plagioclase and quartz. Crystals can vary in size and shape. The texture is nematoblastic, defined by the preferential orientation of amphibole and plagioclase.

The schists are characterized by quartz, biotite, muscovite, and opaque minerals. They are orange, fine-grained, and show a granolepidoblastic texture with a strong planar orientation.

They present a pervasive schistosity, continuous or lentiform, of millimeter to submillimeter thickness (around 1 mm), given by the alternation of dark levels of phyllosilicates (muscovite and biotite) and light levels of quartz. This schistosity is affected by a widely spaced crenulation cleavage of submillimeter to millimeter thickness.

The granitoids are pinkish, medium- to coarse-grained, and can be isotropic or foliated. Foliation is defined by bands consisting of oriented biotite. The texture is medium equigranular phaneritic, and the mineralogy is composed of potassium feldspar, quartz, plagioclase, and biotite. The crystals are subhedral to anhedral, and the color index is leucocratic.

Quartzites can be mylonitized and appear as lenses intercalated with regional migmatites and amphibolites. They are light gray and yellowish when weathered. They have fine to medium granulation, and the texture is granoblastic, defined by the isotropic granular geometry of quartz crystals, where they acquire similar dimensions to each other. Quartz is the essential constituent, accounting for more than 80% of the rock, and, subordinately, micas occur in variable proportions. There may be a thickening of phyllosilicate levels in some portions of the rock. Foliation is moderate to strong or absent (massive structure) and, when it occurs, is due to the alignment of mica crystals and/or stretching of quartz grains. The foliation is pervasive, with millimeter spacing between 0.1 cm and 0.3 cm, with a planar, ductile, and heterogeneous geometry.

The phyllonites present a gray color, becoming reddish-yellow in weathered regions. Commonly, they are mainly composed of biotite, sericite, quartz, and feldspars. The minerals are aligned and slightly stretched. The phyllonites occur strongly banded (ardosian cleavage), showing an alternation of laterally continuous, parallel millimetric to centimetric levels of light colors (quartzous) and dark colors (phyllosilicates). The granulation is fine, with a lepidoblastic texture, where fine crystals of white mica (sericite), biotite, and chlorite are intercalated with beds of granoblastic quartz. The quartz levels are yellowish-gray, finely laminated, and easily disintegrated.

Fault rocks and dikes

The cataclasites are composed of a matrix of very-fine to fine-sized grains and angular polycrystalline fragments. They exhibit shades of gray or beige, and the minerals may be weathered and ground. The mineralogy is formed by quartz, feldspars, biotite, and amphibole. The texture is cataclastic, often fragmented and chaotic, and composed of a mixture of fractured grains with no clear orientation. The structure is typically massive or foliate.

Fault gouge is light to dark gray and characterized by very fine to fine grain. It is formed by crushed and fractured rock, presenting a powdery texture. Its main composition consists of clay minerals and shows a massive structure. The gouge zones can vary in dimensions, ranging from centimeters to meters.

The pseudotachylites are dark and millimetric to centimetric in thickness. They are aphanitic in texture and occur discordantly with the felsic granulites of S_{n-1} foliation. They appear as small, irregular, or serrated veins.

Diabase is dark gray, fine-grained, and formed by pyroxene and plagioclase. The color index is melanocratic, and the structure is massive. The texture is fine equigranular phaneritic, and the alteration is incipient to oxidation.

Lamprophyres are dark or black and have a porphyritic texture, formed by phlogopite phenocrysts dispersed in a fine matrix. They are mainly composed of phlogopite and feldspars.

Structural data

The observation and interpretation of structural data reveal the three-dimensional architecture of rocks and play a fundamental role in the assessment of metamorphosed and deformed

areas. In this item related to structural geology, structural data obtained from the Atuba Complex will be explored.

Ductile structures

The ductile features identified in the area are mainly associated with foliations, mineral stretching, and folds, constituting valuable indicators of the tectonic and metamorphic conditions that shaped the local geology. In the following sections, we will detail each of these features for a more in-depth understanding of the geological context of the study region.

S_{n-1} foliation

Migmatites are characterized by compositional banding on a millimetric or centimetric scale (S_{n-1} surface), featuring alternating felsic and mafic levels. The S_{n-1} foliation (Figs. 6A and 6B), associated with the deformation phase (D_{n-1}), is imprinted in the partially preserved granulitic-derived rocks or the stromatic migmatites with tonalitic leucosome. The penetrative S_{n-1} foliation exhibits an N45W/55NE attitude and is defined by the subparallel orientation of biotite, K-feldspar, and plagioclase, along with the stretching of quartz crystals. It displays a ductile character and a planar nature. In the Schmidt–Lambert stereograms (Figs. 6C and 6D) for the S_{n-1} foliation, dips range from low to high, with a NW-SE direction and a concentration of poles in the SW and NE quadrants. The foliation is affected by open, isoclinic, andptygmatic folds. The limbs exhibit a general direction of N50W/65NE and N55E/80SE. The fold axes (B_{n-1}) are situated in the SE quadrant (Fig. 6E). Mineral stretching lineations (Fig. 6F) have an attitude of N135/35 or N40/40. The cutoff relationship between S_{n-1} and S_n foliations can be observed in the field.

S_n foliation

The S_n foliation (Figs. 7A and 7B), associated with the deformation phase (D_n), is related to high-angle dip shear movements. It may be protomylonitic, mylonitic, or ultramylonitic. It is characterized by the preferential orientation of amphibole and biotite. It is parallel to subparallel with the stromatic migmatite bands, penetrative, locally anastomosed and irregular, heterogeneous, with millimetric to centimetric spacing. It is marked by the presence of mineral flattening, or stretching, reorientation of micaceous minerals, S-C structures, rotated feldspars, moderate recrystallization, macroscopic intrafolial folds, and boudinage structures. It occurs mainly in stromatic-type migmatites with granitic leucosomes.

The structural data on the Schmidt–Lambert diagram show a general NE-SW orientation, with pole concentration in the NW and SE quadrants (Figs. 7C and 7D). The maximum plane is N47E/83NW. Open to isoclinal and intrafolial shear-folds occur. They are millimetric to metric, cylindrical, asymmetric, tilted, and heterogeneous. The folds show limbs with mean attitudes around N26E/76SE and N50E/10SE. The fold axes (B_n) have a NE and SW direction (Fig. 7E). Mineral stretching lineation has mean attitudes of N35/35, N50/5, N110/30, N240/10, and N325/70 (Fig. 7F). They include feldspars, oriented micaceous minerals, and quartz. Boudins are centimeters in size and pink, usually formed by leucosomes. They show the mean directions

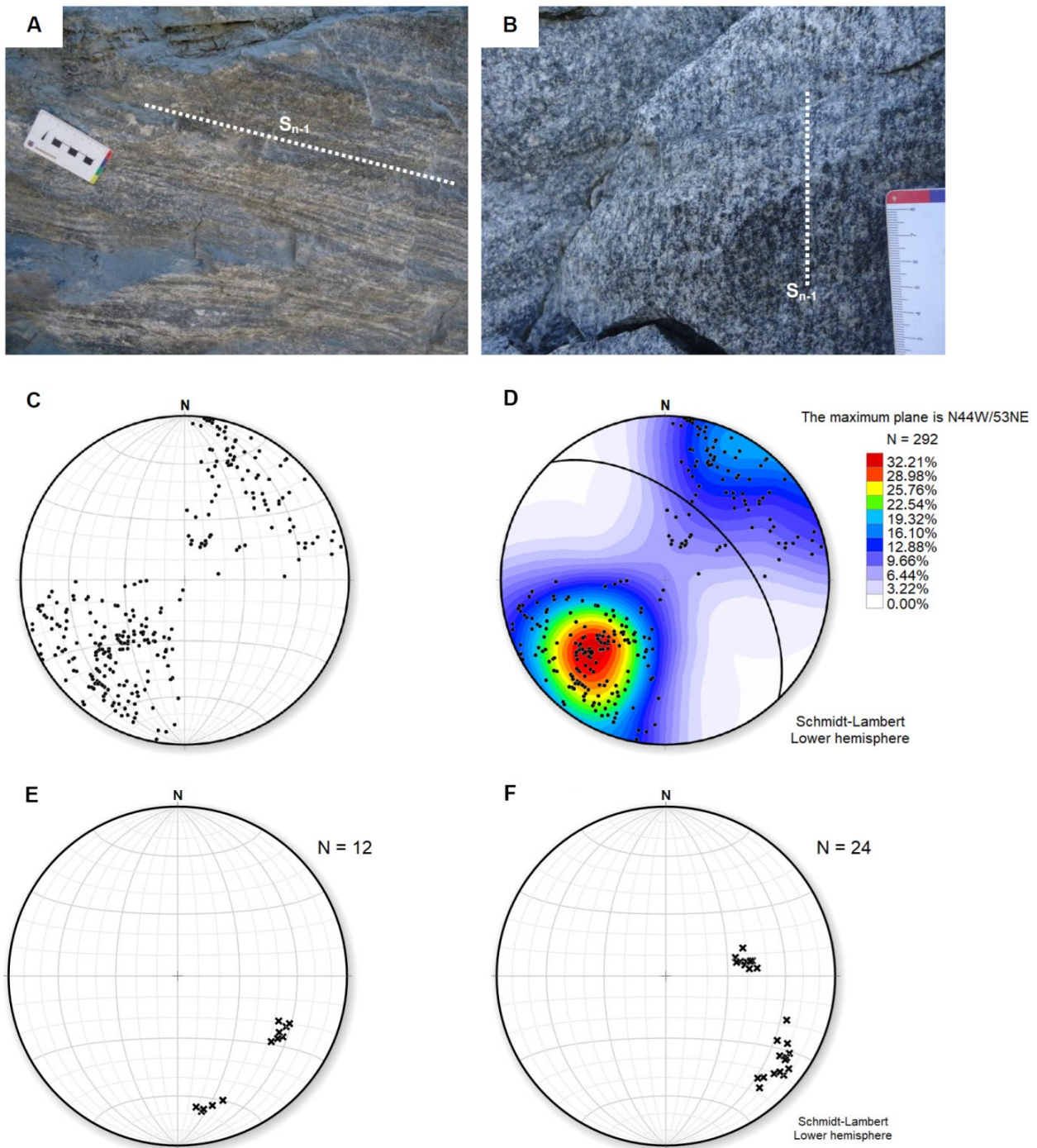


Figure 6. Photographs corresponding to the S_{n-1} foliation and structural diagrams of the S_{n-1} foliation. (A) Macroscopic aspect of the S_{n-1} foliation in the Atuba Complex stromatic metatexites. (B) S_{n-1} foliation with general orientation around N55W/55NE. (C) Stereogram showing the foliation poles. (D) Maximum pole contour diagram. (E) Stereogram of fold axes (B_{n-1}). (F) Stereogram of mineral stretching lineations for S_{n-1} foliation.

N235/65 and N65/10 (Fig. 7G). Kinematic indicators (sigmoidal, oblique foliation, and shear bands) indicated left-lateral movement (Fig. 7H) for the S_n foliation.

Brittle structure framework

In this article, we will explore in detail the strikingly brittle structures in the Atuba Complex. They are characterized by complex patterns of fractures, faults, dikes, and veins in the rocks. The observation and analysis of these structures allowed us to infer crucial information about the direction and magnitude of the tensions that occurred in the area.

Fractures

The fractures observed in the Atuba Complex have two preferred directions: NW-SE and NE-SW (Figs. 8A to 8C). They are cutting migmatites and granulites. NW-SE fractures are open (up to 20 cm) or closed, planar to curvilinear, rough or smooth, parallel between planes, dense (distance between fractures from 5 cm to 30 cm), continuous, pervasive to very pervasive, and filled with calcite, epidote, pyrite, or chlorite. Fracture persistence is metric to decametric. Plane spacing is between 15 cm and 5 m. NE-SW fractures have a continuous, penetrative character with open,

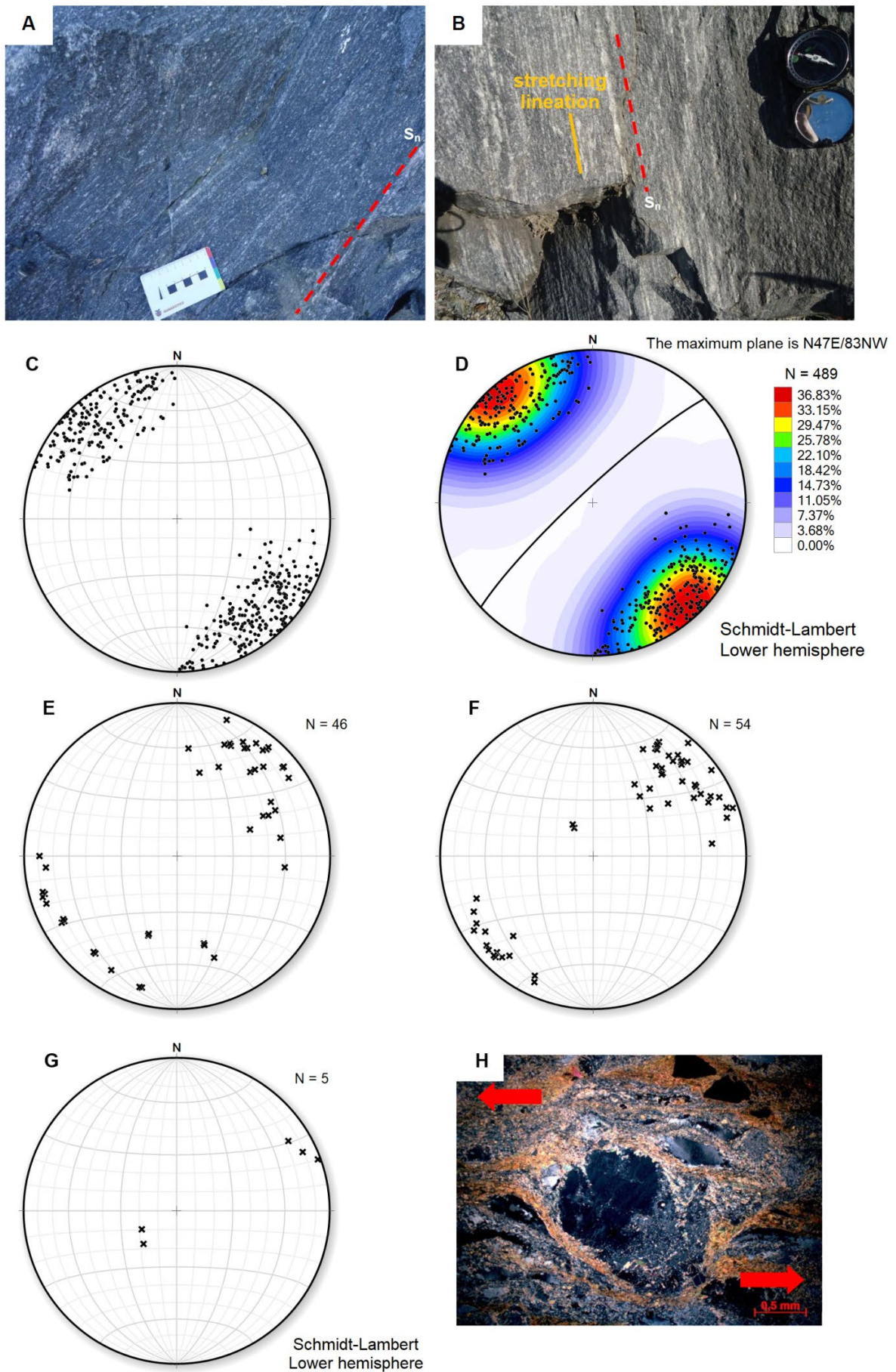


Figure 7. Photographs corresponding to the S_n foliation and structural diagrams of the S_n foliation. (A) S_n mylonitic foliation is defined by the shape and orientation of feldspars and biotite. (B) S_n foliation is characterized by strong stretching of micaceous minerals and quartz-feldspathic aggregates. Down-dip stretching lineation is represented in the XY plane. (C) Pole representation. (D) Maximum pole contour diagram. (E) Stereogram of fold axes (B_n). (F) Stereogram of mineral stretching lineations for S_n foliation. (G) Stereogram of Boudin measurements. (H) Oligoclase porphyroblast with pressure shadows suggesting left-lateral kinematics.

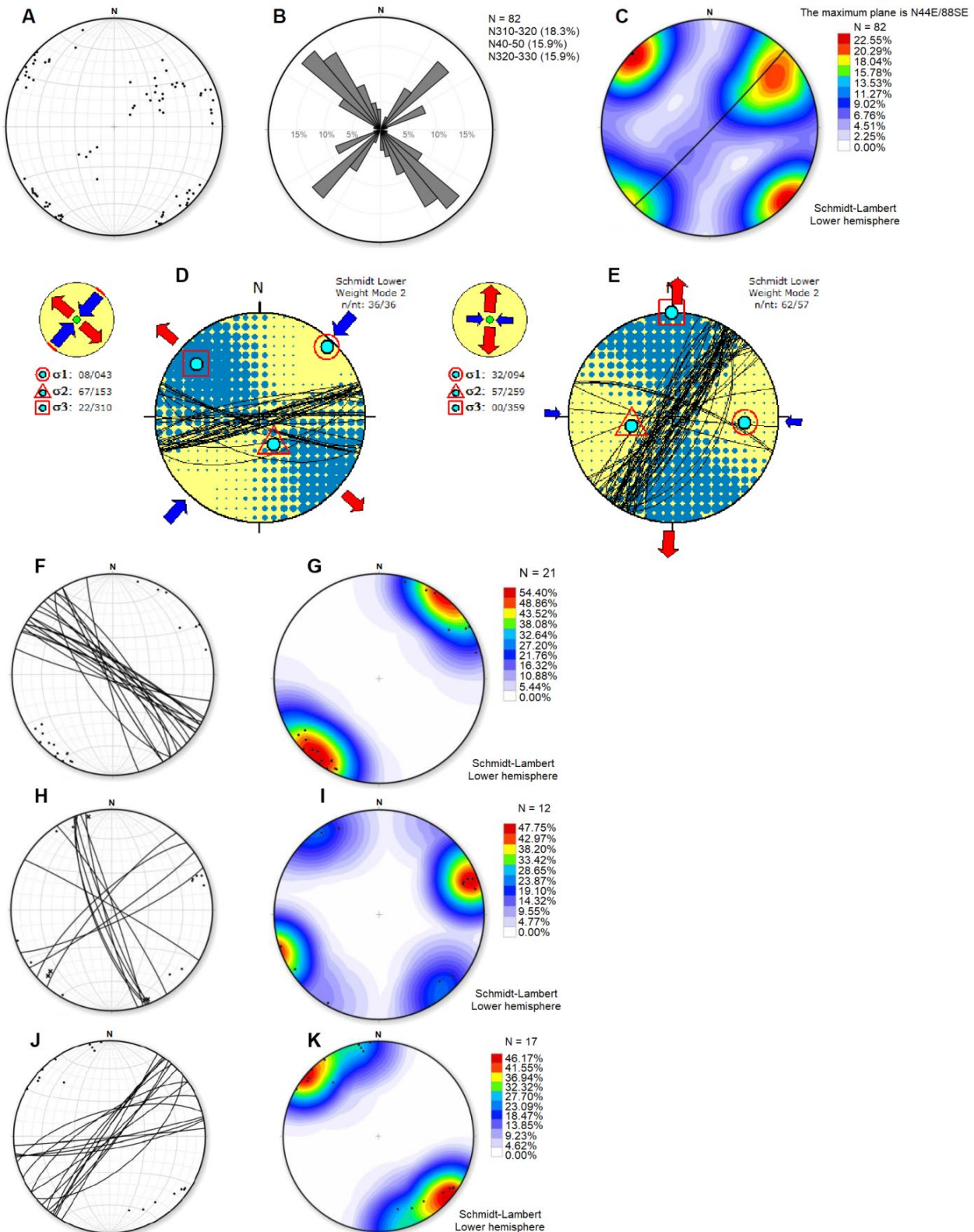


Figure 8. Brittle structural data were observed in the Atuba Complex. Structural diagrams of all fractures visualized in the Atuba Complex: (A) Poles representation. (B) Rose diagram. (C) Poles are isolines. Paleostress diagrams for the transcurrent faults in the working area: (D) Left-lateral. (E) Right-lateral. Structural diagrams of diabase dikes visualized in the Atuba Complex: (F) Cyclographic representation of the planes. (G) Poles are isolines. Structural diagrams of lamprophyre dikes visualized in the Atuba Complex: (H) Cyclographic representation of the planes and their respective poles and striae. (I) Poles are isolines. Structural diagrams of the quartz veins: (J) Cyclographic representation of the planes and their respective poles. (K) Poles are isolines.

rough to partially smooth, straight to curvilinear planes, and carbonate recrystallization, generating an amorphous submillimetric film. They may also be filled with stretched epidote crystals. Fracture persistence is centimetric to

decametric, with density ranging from sparsely dense to dense. Frequently, NE-SW surfaces are subparallel or parallel to the S_n foliation. Fractures of horizontal or subhorizontal character can occur.

Faults

In the Atuba Complex, the presence of different types of faults was verified: inverse, normal, and strike-slip. They are cutting mylonites, granulites, and migmatites. Inverse faults are found locally, ranging in dip angle from low to high, and result in moderate fragmentation or cataclasis. They show distinct failure steps and vertical striations. Its planes are consistent, parallel, smooth surfaces with regular density (distance from 30 to 100 cm), sometimes containing carbonate in their planes. Normal faults exhibit rough, planar to curved planes and breccias. They have a medium to high dip angle, centimeter aperture, and metric persistence. Oblique striations and fault steps are also visible.

The strike-slip faults are on a metric to decametric scale, wide, pervasive, plane, open, dense, with smooth surfaces, and filled with epidote or calcite. These feature nearly horizontal striations and failure steps filled with dark gray material. Faults can be either dextral or sinister in nature. The strike-slip faults show N35E/80SE mean orientation and fault striations in the N200/10 direction. Flowering structures, positive or negative, are rarely found.

The paleostress analysis performed on the structural data of left-lateral (Fig. 8D) and right-lateral (Fig. 8E) transcurrent faults allowed the identification of a NE-SW sigma 1 associated with a near-vertical sigma 2 and a NW-SE-oriented sigma 3 for the left-lateral faults, and an E-W compressive SH_{MAX} and an N-S distensive SH_{MIN} for the right-lateral faults. The left-lateral transcurrent faults were superimposed by the right-lateral transcurrent faults, and their kinematic indicators were erased or masked by right-lateral movement, making identification of the left-lateral kinematics complex. A spoon-like kinematic indicator was observed at the Atuba Complex, suggesting left-lateral movement. Well-defined striae and steps are noted.

Dikes and veins

The dikes and veins date back to the Cretaceous period and are commonly observed and associated with the migmatites in the area. The diabase dikes appear fractured or faulted, with striation and step generation. They may present carbonate vesicles and veins in their extremities. The thickness of the dikes is variable, ranging from 2 to 20 m. All measurements of the dikes' orientation can be seen in Figs. 8F and 8G. Lamprophyre dikes are up to 3 m thick and may show a lenticular or anastomosed-shape appearance. There are faults and fracture planes that cut the dikes. The Schmidt-Lambert diagrams (Figs. 8H and 8I) show NW-SE and NE-SW strikes as the lamprophyre dikes' main directions. Measurements of quartz veins can be seen in Figs. 8J and 8K.

Petrography

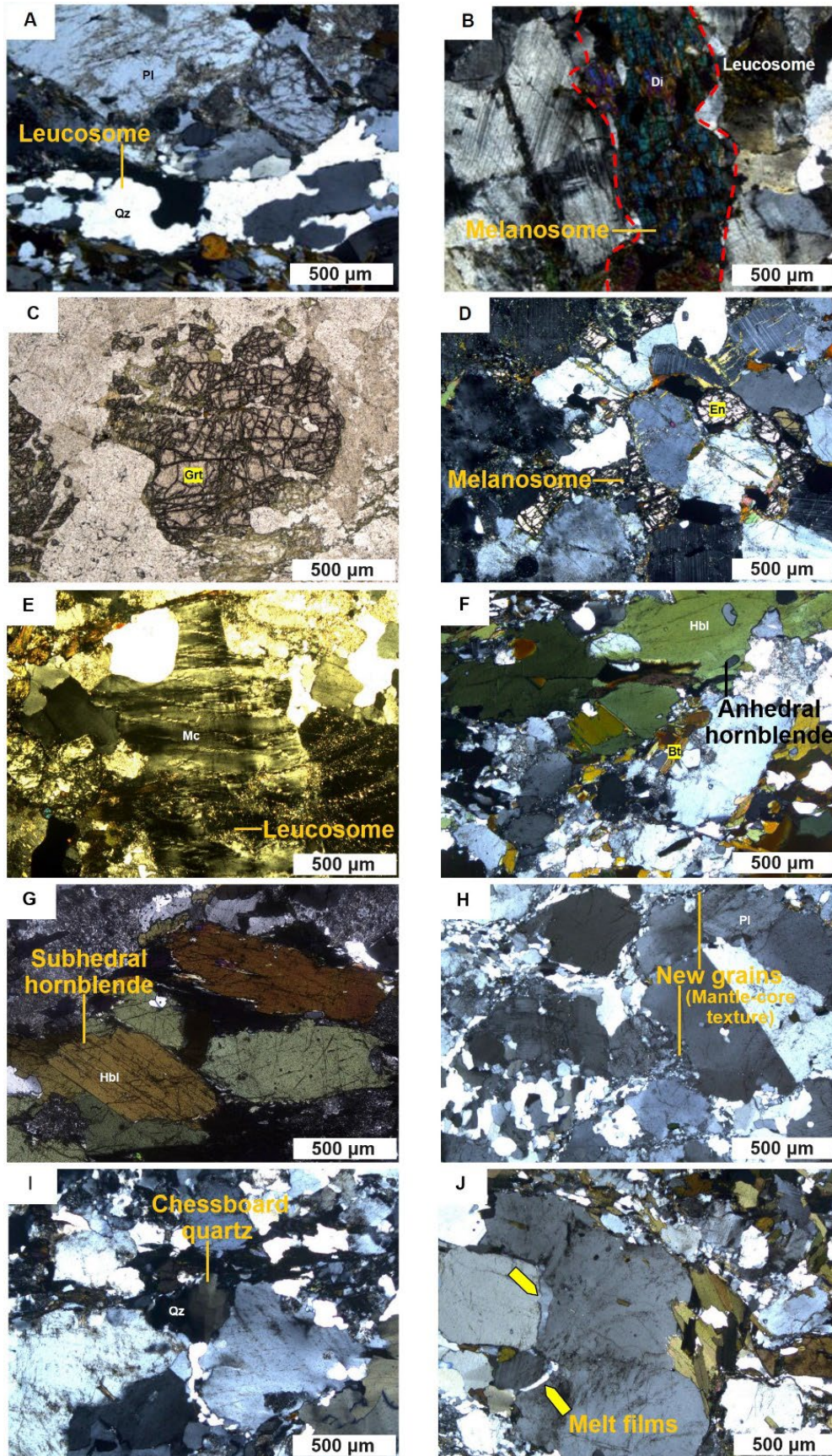
In this section, only the rocks that occur in greater proportion in the Atuba Complex will be addressed. Patch migmatite consists mainly of plagioclase and quartz, with rare garnet, hornblende, and biotite crystals occupying the core and leucosome boundaries. Plagioclase crystals are prismatic subhedral, medium to coarse, and occur moderately saussuritized. They show undulose extinction and mechanical twinning.

Quartz crystals are fine to medium, granular anhedral, and show undulose extinction, subgrains, and bulging-like features. Garnet crystals are medium to coarse, anhedral, and microfractured. Hornblende crystals are greenish, fine to coarse, anhedral, with undulose extinction and microfractures. Biotite crystals are fine to medium, anhedral to subhedral lamellar, strongly oriented, and anastomosed. They have undulose extinctions and kink bands.

Stromatic migmatites occur with two types of leucosomes and melanosomes. The first is formed by white leucosomes, and the second by pink leucosomes. White leucosomes (Fig. 9A) show andesine, quartz, and microcline. Andesine is fine to coarse, anhedral to subhedral prismatic, and shows undulose extinction, subgrains, and new grains. Quartz grains are fine to medium, anhedral, and have no preferred orientation. They have undulose extinctions and subgrains. The boundaries are curvilinear and lobed. The microcline is fine to coarse, anhedral to subhedral, and exhibits perthite in flame and undulose extinction, as well as new grains. The melanosome can occur on both sides or only on one side of the leucosome. It shows fine granulation and is weakly oriented. It may show diopside (Fig. 9B), garnet (Fig. 9C), enstatite (Fig. 9D), and plagioclase, in addition to biotite and hornblende.

The mesocratic residual neosome has fine- to medium-sized grains and consists of andesine, quartz, biotite, and hornblende. The accessory minerals are microcline, apatite, opaque minerals, zircon, titanite, allanite, and muscovite. The secondary minerals are pennine, carbonate, epidote, and sericite. The andesine crystals are poorly stretched and exhibit undulose extinction, kink bands, subgrains, deformation twinning, albite-pericline-type polysynthetic twinning, myrmekite, and new grains. Quartz crystals show undulose extinction, subgrains, deformational bands, chessboard pattern texture, lobate grain boundaries, and microfractures. They may show a melt pool, cusp-shaped terminations, and lobate boundaries with feldspar crystals. Biotite crystals are characterized by undulose extinction, kink bands, and deformation bands. Hornblende crystals have undulose extinction, subgrains, rare new grains, and microfractures.

The pink leucosome bodies exhibit fine- to coarse-sized graining and are formed by K-feldspar, quartz, and plagioclase crystals (Fig. 9E). They exhibit undulose extinction and new grains. The leucosome is incipiently bound by biotite- and hornblende-rich melanosomes. The peritectic minerals may show anhedral (Fig. 9F) or subhedral to euhedral (Fig. 9G) forms and rectilinear or irregular contacts. The residual neosome consists of mesocratic, gray, quartz-feldspathic gneiss with bands of millimetric to centimetric thickness. The average composition consists of oligoclase, quartz, biotite, hornblende, and accessory minerals such as apatite, opaques, chlorite, zircon, and titanite. The oligoclase crystals show undulose extinction, myrmekite, deformation twinning, and new grains (Fig. 9H). Quartz crystals show undulose extinction, kink bands, chess-board pattern texture (Fig. 9I), and subgrains. Occasionally they comprise melt films (Fig. 9J), interstitial quartz, cusp-shaped, and melt pools. Biotite crystals have undulose extinction and curve-shaped cleavages. Hornblende crystals can have a rounded or



Di: diopside; Grt: garnet; En: enstatite; Mc: microcline; Bt: biotite; Hbl: hornblende; Pl: plagioclase; Qz: quartz.

Figure 9. Photomicrographs of stromatic metatexites. All thin sections have cross-polarized light, except Figure C. The arrows correspond to the microstructures analyzed in the figures. (A) Tonalitic leucosome consisting of andesine and quartz crystals with irregular contacts and subgrain formation. (B) Diopside crystals with serrated contacts and a tonalitic leucosome consisting mainly of andesine and quartz. (C) Strongly fractured garnet crystal with coarse graining. (D) Melanosome consisting of enstatite. (E) Microcline-oligoclase-quartz-rich leucosome. (F) Peritectic crystals consisting of anhedral hornblende with cusp-shaped terminations and fine- to medium-grained biotite lamellae. (G) Melanosomes are formed by subhedral and medium-grained hornblende. (H) Mantle-core texture oligoclase. (I) Chessboard pattern texture in quartz crystal. (J) Melt films between coarse-grained oligoclase crystals.

eroded appearance and, together with titanite, mainly exhibit closed microfractures. Hornblende is also characterized by a corona-like texture. Chlorite crystals have undulose extinction as a deformation feature.

Mylonitic migmatites are composed of oligoclase/andesine, quartz, muscovite, biotite, and microcline. Accessory minerals are hornblende, opaques, apatite, and zircon. Secondary minerals are carbonate, epidote, chlorite, and sericite. The leucosome bands show centimetric to metric thickness and are composed of K-feldspar, quartz, and plagioclase. The minerals (plagioclases, quartz, biotite, and hornblende) define S_n foliation. The melanosome is thin, dark gray-colored, and formed by biotite and hornblende. The oligoclase/andesine crystals show deformation twinning, kink bands, and new grains. Quartz crystals exhibit lobate grain boundaries, ribbons, undulose extinction, and subgrains. Muscovite crystals have curve-shaped cleavages and undulose extinction. Biotite crystals have undulose extinction, stretching, and anastomosed shapes. The microcline crystals have undulose extinction, new grains, and microfractures. Hornblende crystals are characterized by undulose extinction and microfracture.

The granulites consist of andesine, enstatite, diopside, garnet, hornblende, quartz, microcline, biotite, and opaques. The accessory minerals are formed by zircon, apatite, and allanite. Secondary minerals are epidote, chlorite, calcite, and sericite. The prismatic minerals show incipient orientation. Quartz-feldspathic aggregates show interlobate contacts. Cusp-shaped melt pools were observed, showing thin, sharp edges, and penetrating along the boundaries of adjacent grains. The minerals in contact are slightly rounded, suggesting corrosion. Also noted are localized melt films along grain boundaries (Figs. 10A and 10B) and microcline with interstitial character (Fig. 10C). Garnet crystals may show many fractures (Fig. 10D), and enstatite crystals may show corona-like reaction features, with green hornblende surrounding medium-sized grains (Fig. 10E). Diopside crystals occur moderately altered (Fig. 10F), with irregular contacts, no orientation, and medium- to coarse-grained. Opaque minerals are fine, anhedral to subhedral, interstitial, and associated with mafic minerals in the rock.

The amphibolites are composed of hornblende, andesine, and quartz. Hornblende crystals are medium-equigranular, prismatic subhedral, with straight and curvilinear contacts. The hornblende partially defines S_n foliation. Andesine crystals are medium-equigranular, anhedral to subhedral prismatic, with a preferred orientation. They have straight and irregular boundaries. They show undulose extinction and kink bands, and quartz inclusions may occur. Quartz crystals are fine equigranular, granular anhedral, without preferential grain orientation. The contact between the crystals is straight or curved.

Granitoids are formed by quartz, oligoclase, microcline, biotite, opaques, and chlorite. Quartz crystals are fine to medium inequigranular, anhedral granular, and have no preferred orientation. Boundaries are straight and curved. They show undulating extinction as a deformational feature. Oligoclase crystals are fine to medium, anhedral to subhedral prismatic, and moderately saussuritized. There are inclusions that are opaque. Oligoclase crystals show myrmekites and zoning. Microcline

crystals are fine to medium inequigranular, anhedral to subhedral, and exhibit undulating extinction and pertites. There are quartz and opaque inclusions. Biotite crystals are thin, subhedral, have wavy extinction, and have poor preferential orientation. They may occur at anastomosed levels, surrounding oligoclase or microcline crystals. Opaque crystals are fine, anhedral, and associated with biotite. They do not have a preferred orientation. Chlorite crystals are very fine to fine, anhedral, and interstitial in disposition.

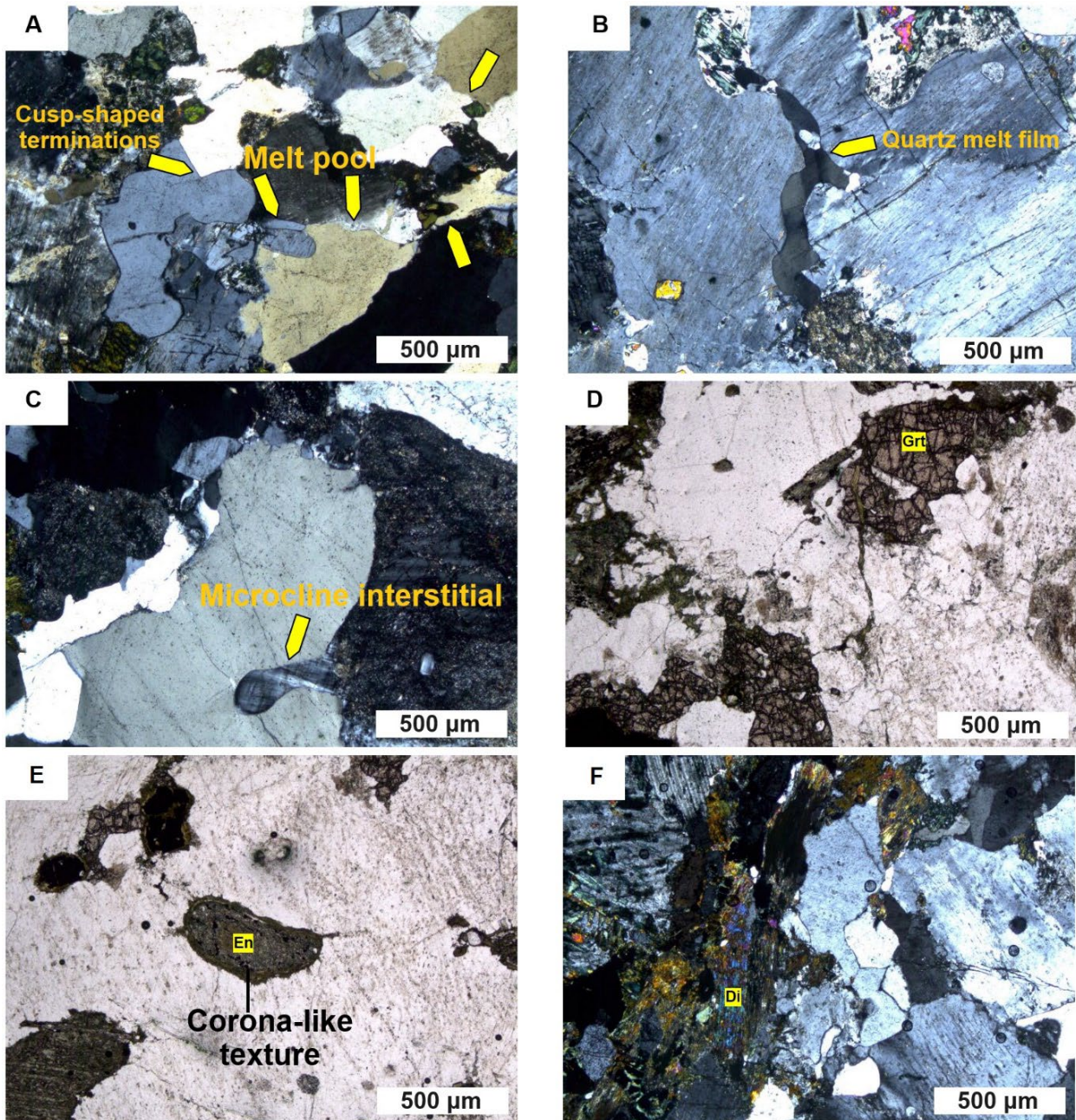
The quartzites are fine- to medium-grained and present quartz, biotite, muscovite, and opaques. Quartz is inequigranular, granular anhedral, very fine to fine-grained, and stretched in the direction of S_n foliation. It shows undulating extinction and preferential orientation. Biotite crystals are thin, subhedral, and oriented according to the main foliation direction (S_n). They occur in rectilinear contact and are stretched, with opaque inclusions. Muscovite is equigranular, very fine, lamellar subhedral, and strongly stretched in the direction of S_n foliation. The contacts are straight and irregular. Opaque minerals are fine, anhedral, and occur without orientation. Contacts are straight-to-locally serrated. Occur incipiently altered to iron oxide. The texture is granoblastic or granolepidoblastic. Foliation is moderate to strong and is defined by the alignment of mica and/or stretching of quartz grains. It is penetrative, ductile, heterogeneous, and shows millimeter spacing and planar geometry.

Schists are formed by quartz, biotite, muscovite, plagioclase, and opaque. Quartz crystals are inequigranular, fine to medium, anhedral granular, and elongated. Its edges are partially serrated and straight. Subgrains and undulating extinction occur, with opaque inclusions. Biotite crystals are thin, subhedral, and oriented. They occur in mutual and rectilinear contact with quartz and muscovite crystals. They feature quartz and opaque inclusions. Muscovite crystals are fine, subhedral, and elongated. They are slightly crenulated, with straight contact. Plagioclase crystals are prismatic, medium, and oriented subhedral. They are in rectilinear and irregular contact with the other minerals in the rock. Opaque crystals are fine, granular anhedral, with interlobed contacts. They occur dispersedly without preferential orientation.

Cataclastic rocks, dikes, and veins

The phyllonites are dark, fine-grained, and formed by biotite, hornblende, oligoclase, and quartz. The biotite crystals are fine- to medium-grained, subhedral lamellar, moderately oriented, and fractured. Undulose extinction and curve-shaped cleavages occur. Oligoclase crystals show undulose extinction and deformation twinning. Quartz crystals show intracrystalline subgrains, undulose extinction, and intracrystalline fractures. They do not exhibit preferential orientation. The phyllonites show foliation characterized by the subparallel orientation of the mafic minerals and may be associated with brittle shear zones.

Cataclasites show oligoclase, quartz, microcline, chlorite, opaques, carbonate, and iron oxide. They show evidence of fracturing and comminution. The oligoclase crystals show undulose extinction, closed or carbonate-filled microfractures,



Qz: quartz; Grt: garnet; En: enstatite; Di: diopside.

Figure 10. Photomicrographs of felsic granulites. All thin sections have cross-polarized light, except Figures D and E. The arrows correspond to the microstructures analyzed in the figures. (A) Melt pool crystallized in lobate quartz grains, exhibiting films between minerals and sometimes cusp-shaped terminations, with consumed feldspars around. (B) Irregularly shaped quartz melt film at contact with feldspar crystals. (C) Microcline with interstitial appearance between andesine crystals. (D) Medium-sized, intensely fractured garnet (almandine) with irregular contacts and a slightly skeletal appearance. (E) Enstatite with a corona-like texture. (F) Altered medium-grained diopside in the contact between andesine and opaque crystals.

and microfaults. Quartz crystals have undulose extinction, intracrystalline subgrains, microkinks, microfaults, and closed microfractures. Microcline crystals show undulose extinction, microfaults, and closed conjugate and carbonate-filled microfractures. The chlorite and carbonate crystals have microfaults and microfractures.

The diabase and gabbro dikes are dark gray and composed of augite and labradorite. Carbonate is observed as a secondary mineral. The color index is melanocratic, the texture is subophytic to intergranular, and the structure is massive. The augite crystals display an anhedral to subhedral morphology and

do not exhibit any distinct preferred orientation. Inclusions of labradorite and opaques occur. The labradorite crystals are subhedral to euhedral and show no preferential orientation. Inclusions of opaques occur. The carbonate crystals are anhedral and have curved and irregular edges.

Kersantite lamprophyre dikes are formed by phlogopite, oligoclase, serpentinized olivine, opaques, carbonate, and volcanic glass. They have a flow or massive structure. The granulation is fine to coarse.

There are white, weakly- to strongly-fractured quartz veins with a thickness of 0.1–30 cm. They occur parallel to

the migmatites in the S_n foliation. Quartz crystals are fine- to medium-grained, anhedral, with serrated and curved contacts. They exhibit subgrains, stretching, and undulose extinction. The epidote veins are arranged parallel or discordant to the compositional banding. They are green and centimetric in thickness. The crystals are very fine- to medium-grained, unequigranular, and anhedral, with irregular boundaries. They show undulose extinction and microfractures. Carbonate veins are discordant to the foliation, white, and millimetric to centimetric in thickness. Carbonate crystals are anhedral, very fine to fine-grained, with irregular contacts. They may show undulose extinction. Chlorite veins are green, submillimetric, and have very fine to fine-grained crystals. They appear to be cutting the migmatite foliation.

DISCUSSION

The working area is in Curitiba City and surrounding regions. The Atuba Complex (Siga Junior *et al.* 1995) is formed essentially by migmatites of various morphologies and associated rocks.

The Atuba Complex rocks are formed by two migmatization phases. They were defined based on field, petrographic, structural, microstructural, and geochronological data. The ages of the migmatization phases were taken from the geological literature (Table 1), carried out by several authors (Siga Junior 1995, Siga Junior *et al.* 1995, 2007, Kaulfuss 2001, Sato *et al.* 2003, 2009). The first phase (2100–2400 Ma, Siga Junior *et al.* 2007) is formed by tonalitic white, foliated, folded leucosomes with small proportions of pinkish leucosomes (granitic). The melanosome is composed of orthopyroxene, clinopyroxene, and garnet. It is observed in stromatic metatexites and felsic granulites. The second phase (620–600 Ma, Siga Junior *et al.* 2007) corresponds to granitic and pinkish, massive to foliated leucosomes, with smaller amounts of white (tonalitic) leucosomes. The melanosomes are formed by biotite and hornblende. This phase is marked by stromatic metatexites. Generally, the leucosomes of the first and second phases are parallel to the compositional banding (S_{n-1}) or the mylonitic foliation (S_n).

In the Atuba Complex, evidence for two separate migmatization processes becomes apparent through careful analysis of the geological structures and their cross-cutting relationships. The key to this distinction lies in the clear organization of the different phases of migmatization and the cutoff relationships that exist between them. The first phase of migmatization, clearly identified, presents specific characteristics that distinguish it from the second phase. These characteristics may include unique mineralogical compositions, particular foliation patterns, and specific spatial distributions. When examining the migmatite rocks resulting from the first migmatization, we can observe a cohesive and penetrative structural organization. The second phase of migmatization, on the other hand, is recognized by the presence of distinct characteristics that differentiate it from the first. Careful analysis reveals that the structures related to this second migmatization cut the structures of the first at different angles. This phenomenon is fundamental to establishing the temporal

sequence of geological events, clearly indicating that the second migmatization occurred after the formation of the first. The shear relationship between the two migmatization phases can be evidenced by veins or shear zones that intersect the pre-existing structures. Interpreting these shear relationships provides a deeper understanding of the geological evolution in the Atuba Complex. These observations suggest that geological conditions have changed over time, allowing two migmatization events to occur.

First migmatization phase

Stromatic migmatites and felsic granulites are characterized by high-temperature minerals such as enstatite, diopside, garnet, and andesine (Yardley 2004, Bucher and Grapes 2011). They correspond to the granulite facies and can be foliated or not. Silva (2005) also witnessed garnet crystals, possibly as melanosome peritectic minerals that occur with the granodioritic to tonalitic leucosomes from the Artecipe quarry.

The stromatic migmatites show andesine and microcline with new grain features; quartz with chess-board pattern texture and irregular, lobate edges suggesting grain boundary migration (GBM); and hornblende with rare, very-fine-sized new grains located at its boundaries. The leucosome is essentially tonalitic and defined mainly by plagioclase, quartz, and potassium feldspar. The microstructures indicate the action of intracrystalline mechanisms by dislocation creep and dynamic recrystallization processes by GBM for quartz and bulging or mantle-core texture for feldspars, evidencing temperatures above 500°C (Stipp *et al.* 2002). The chess-board pattern texture observed in quartz crystals occurs at temperatures near granite solidus (Mainprice *et al.* 1986, Kruhl 1996), diagnosing deformation processes above 600°C. Hornblende shows dynamic recrystallization at temperatures above 700°C (Passchier and Trouw 2005).

Felsic granulites are characterized by high-temperature minerals, such as enstatite, diopside, garnet, and andesine. They correspond to the granulite facies and can be foliated or not. Quartz and feldspars present interlobate contacts, often with a cusp-like shape or interstitial aspect. The enstatite crystals may exhibit hornblende edges (corona-like). There are films of melt along the edges of the medium-sized grains. The observed minerals and microstructures indicate temperatures above 850°C. Reactions of corona are highly significant as they delineate preserved reactions within a rock's structure. These coronas can arise from solid-state metamorphic reactions, for instance, interactions between solids and fluids and partial melting. In metamorphic rocks, they can be triggered by changes in pressure-temperature conditions as well as interactions with external fluids, which are more common in high-grade metamorphic rocks (e.g., granulites) and ultramafic rocks (Vernon 2004). Basei *et al.* (1999) described cores of charnockite-enderbite composition, distributed mainly in the northeastern region of the Curitiba Terrane. Siga Junior (1995) and Siga Junior *et al.* (1995) observed granulitic gneisses northward and southward of Curitiba city, containing andesine-labradorite, garnet, diopside, and orthopyroxene, as did Fuck *et al.* (1967), who noted diopside in some Atuba Complex gneisses.

Second migmatization phase

The second migmatization phase constitutes stromatic migmatites formed by granitic leucosomes with microcline and oligoclase crystals with aspects of new grains by bulging and quartz recrystallized by GBM; melanosome characterized by hornblende and biotite (crystals with undulose extinction and kink bands); and mesocratic residual neosome composed mainly of plagioclase (oligoclase with undulose extinction, myrmekite, deformation twinning with conical-shaped terminations and new grains), quartz (irregular grains with undulose extinction, kink bands, subgrains and dynamic recrystallization by GBM), biotite (lamellae with undulose extinction and curve-shaped cleavages) and hornblende (medium- to coarse-grained crystals with closed microfractures). The residual neosome is medium- to coarse-grained and locally shows narrow films of quartz or feldspars (leucosome) along the crystal contacts, interpreted as pseudomorphs replacing the spaces originally occupied by melt, indicating that not all the generated liquid was extracted. Microkinks occur as isolated structures in quartz and are probably associated with cataclastic aspects at dislocation tangle sites (Tullis and Yund 1987) and suggest dislocation glide (Passchier and Trouw 2005). In this case, they are posterior structures to the Atuba Complex second migmatization phase and possibly comprise a phase of brittle deformation.

Silva (2005) calculated the temperatures at the Atuba quarry from Holland and Blundy's (1994) method and obtained temperatures (Hbl-Pl) of the mesocratic residual neosome between 690 and 783°C, and pressures on the order of 6.14–7.60 kbar. For the Artecipe quarry, they found temperatures around 710–752°C and estimated pressures between 6 kbar and 7.4 kbar, corroborating the results obtained at the Atuba quarry. The same author calculated the saturation temperatures in Zr and P for the Atuba quarry leucosomes using zircon and apatite crystals. The leucosomes TZr obtained occur around 663°C. For the P saturation temperature, the results are around 715°C.

Protomylonitic to ultramylonitic migmatites exhibit oligoclase or andesine and microcline with new grain features and quartz formed by GBM, suggesting temperature of 500°C (Stipp *et al.* 2002). Quartz also occurs as new grains by subgrain rotation (temperatures of 400–500°C, Stipp *et al.* 2002) and bulging at temperatures of approximately 280–400°C (Schmid and Handy 1991, Stipp *et al.* 2002), probably due to exhumation effects and retrograde metamorphism that occurred in the final phase of deformation of the Atuba Complex and may be related to the Curitiba Shear Zone (Gonçalves 2012, Cabrita 2015, Conte *et al.* 2020). The mylonite migmatites show dislocation creep mechanisms. Faleiros *et al.* (2016) described deformation mechanisms in the Serra do Azeite Shear Zone and found GBM processes with bulging superimposition (BLG) in the residual neosome, GBM with subgrain rotation superimposition (SGR) in the granitic leucosome, and SGR in retrograde mylonitic orthogneiss. In this case, no SGR features with BLG superimposition were observed. Conte *et al.* (2020) observed rocks recrystallized by bulging in the southern portion of the Lancinha Shear Zone and by subgrain rotation and GBM in the northern portion of the zone. The processes

of recrystallization by bulging or subgrain rotation are considered the main recrystallization mechanisms. The present work corroborates the data found in Conte *et al.*'s (2020) research.

Microstructures

Partial melting microstructures occur in the first and second migmatization phases. Magmatic flow can be defined as the deformation by melt displacement, with consequent rotation of rigid crystals, without sufficient interference between crystals to cause plastic deformation (Paterson *et al.* 1989). They are characterized by quartz and feldspar grains with interstitial or cusp-like shapes, lobate boundaries of quartz grains, melt films that have crystallized into quartz or feldspar crystals, preferential orientation of biotite crystal shape, rare plagioclase crystals with rectilinear boundaries, and minerals with an absence of intracrystalline ductile deformation, suggesting that they were crystallized from magma or that the microstructure was erased. Sharped films along crystal faces can be noted in experimental melts under dynamic conditions (Jin *et al.* 1994), and cusp- or lobular-shaped boundaries are understood as reservoirs of crystallized melt (Jurewicz and Watson 1984). Plagioclase films between quartz or potassium feldspar grains probably have a more albite composition than the original grains. Potassium feldspar crystals with cusp-like edges may represent a component crystallized from fusion (Sawyer 1999, 2001).

The submagmatic microstructures show evidence of intracrystalline deformation and occur in a generalized way (first and second migmatization phases) in the Atuba Complex. They exhibit undulose extinction, deformation bands, subgrains, deformation twinning, kink bands, chess-board pattern structure, anastomosed fine-grained foliation, elongation of recrystallized aggregates, ribbons, myrmekites, microcline twinning, flame perthite, boudinage of resistant minerals, heterogeneous deformation with local mylonitic zones, recrystallized tails in porphyroclasts, new grains in plagioclase suggesting temperatures above 450°C (Voll 1976), recrystallized potassium feldspar with exsolution lamellae, relatively calcic plagioclase with myrmekite, S-C structures, and recrystallization in hornblende.

The coexistence of microstructures observed in the Atuba Complex suggests that the migmatites of the two migmatization phases and the granulites of the first phase were deformed under high temperature in a transitional rheological state between suspension flow and grain-supported flow. The leucosomes found in banded lithotypes in the first and second migmatization phases probably started as pocket melts, which progressively coalesced and migrated laterally, concentrating across the compositional banding and parallel to the S_{n-1} or S_n foliation. Generally, the leucosomes show regular thickness and continuity, which favors movement, exhibiting a lower proportion of mafic minerals than the residual neosome. The leucosomes observed in migmatites with dilation structures (second migmatization phase) possibly formed as isolated pocket melts and were in low-pressure sites due to the brecciation that was driven by deformation and by the massive structure of the rocks.

There are white and pink leucosomes in both migmatization phases, with a predominance of white leucosomes in the first phase and a predominance of pink leucosomes in the second phase. The composition, color, and minerals that make up the leucosomes in the two phases are similar. The difference between the white and pink leucosomes of the first and second phases is the mineralogical aspect of the melanosome that accompanies the leucosome in its edges, being that in the first phase, the melanosome presents pyroxene and garnet, and in the second phase, it shows hornblende and biotite, besides the shape of the leucosome (more defined and rectilinear in the first phase and diffuse in the second) and the well-developed foliation in the first phase and less marked or absent in the second phase. The pinkish leucosome of the second phase can also be pegmatitic, something not noticeable in the first phase. It regularly shows malformed, incipient, or absent melanosomes and mafic selvages.

Through petrographic techniques, the main melting reactions during the Atuba Complex migmatization were determined. Water-fluxed melting reactions are different from dehydration melting reactions, mainly with respect to the presence, type, and composition of peritectic minerals and melts; melting temperatures; inclination of the solidus curve; and initial water content of the melt. In dehydration melting reactions, all the water is derived from hydrated minerals, and the produced melt is subsaturated in water, with incongruent reactions at higher temperatures, in contrast to water-fluxed melting reactions, where the melt can be rich or saturated in water, generating congruent responses at lower temperatures (Weinberg and Hasalová 2015).

Partial melting is a crucial geological phenomenon that occurs under specific conditions, especially in metamorphic environments. Migmatization marks the beginning of this process, occurring when temperature and pressure conditions exceed the stability limit of certain minerals, leading to a partial melting of the rocky material. The dehydration-fusion reaction is an essential component of this process. It occurs when rocks containing hydrated minerals are subjected to metamorphic conditions, resulting in the release of water. The presence of water is essential to reducing the melting point of minerals, thus facilitating partial melting. The first phase occurred by hornblende breakdown, with the reaction: $Hbl + Pl = Cpx (+ Grt + Opx + Amp) + melt$. During the first partial melting event, the peritectic phases also play a crucial role. The peritectic minerals generated are plagioclase, orthopyroxene, clinopyroxene, and garnet. Leucosomes that have anhydrous (peritectic) minerals are more likely to be a product of dehydration melting (Brown 2013). The composition of the melt observed in the Atuba Complex rocks is plagioclase-rich, with a tonalitic composition. Dehydration melting of amphibole occurs at temperatures between 850 and 900°C (Wyllie and Wolf 1993, Wolf and Wyllie 1994). Regarding the garnet crystals, increasing amounts of water reduce their stability (Gardien *et al.* 2000), while pyroxene stability is controlled by temperature, pressure, rock composition, and water content (Patiño Douce 1996). In the absence of low amounts of water, the formation of Opx or Cpx over amphibole is favored (Weinberg

and Hasalová 2015). Migmatization, dehydration fusion reaction, and formation of peritectic phases are specific terms that describe distinct stages of this complex partial fusion event. These phases develop in response to changes in the chemical composition of the rock during the melting process and subsequent cooling. These processes are intrinsically linked and play a crucial role in the evolution and transformation of rocks in metamorphic environments.

In the second migmatization phase, there was the participation of free water (water-fluxed melting) as a reactant in upper amphibolite facies, and probably the reaction $Pl + Kfs + Qtz + H_2O \pm Ms \pm Bt \pm Hbl = liquid$, producing hydrated peritectic phases such as hornblende and biotite, according to the criteria proposed by Sawyer (2001, 2008). The crystals are well formed and in contact with quartz and feldspar grains. These reactions typically preferentially consume potassium feldspar, which tends to be depleted in the residual neosome. Consequently, the leucosome formed is potassium feldspar-rich (granitic to alkali-feldspar granitic composition). Leucosomes bearing mica and hornblende without anhydrous (peritectic) minerals are more likely to be the product of a water-fluxed melting reaction (Brown 2013). Experiments on granites and tonalites under water-saturated conditions and 1–3 kbar showed eutectic melts with peritectic hornblende (Gibbon and Wyllie 1969). Several experiments, such as those by Johnston and Wyllie (1988) and Gardien *et al.* (2000), suggest that the presence of hornblende crystals indicates the addition of external aqueous fluids during partial melting. Other factors that highlight water-fluxed melting as the main migmatization process of the second phase are the large melt volume, meso- and microstructures, leucosome morphology, melting reactions, nature of the peritectic phases, and temperatures estimated at 700°C. Water-fluxed melting reactions of pelites and granites initiate melting around 620–650°C at normal crustal pressures (Weinberg and Hasalová 2015).

Plagioclase, hornblende, and biotite crystals with rounded and eroded shapes were categorized as reactive minerals not fully depleted during melting. Crystals of hornblende and biotite (reaction by water-fluxed melting) with subhedral or euhedral shapes were interpreted as peritectic minerals. On the microscale, anhedral crystals of biotite and hornblende, locally cusp-shaped, and inclusions of rounded quartz and feldspar crystals also occur. The biotite and hornblende with anhedral or cusp-like shapes were interpreted as minerals that formed during the early stages of partial melting with no room for crystallization. The subhedral or euhedral forms of these crystals were understood to be generated during advanced stages of melting, with free space for crystallization.

The leucosomes of both migmatization phases suffered an important structural control, responsible for the generation, accumulation, migration, and extraction of large volumes of liquid, and the partial melting was also influenced by the rocks' anisotropy. The Atuba Complex lithotypes show anatexis features, with the generation of large volumes of neosomes. The migmatites located in the northern part of the area might have suffered some influence from the Anhangava Granite, Graciosa Granite, and Marumbi Granite, while the rocks located in the

southern part might have been influenced by the Agudos do Sul Granite. Due to their Neoproterozoic to Cambrian age, these alkali-granitic suites might have acted in the second migmatization phase. In water-fluxed melting reactions, the water can be derived from shear zones, which serve as conductors in the system, such as the Lancinha Shear Zone, the Curitiba Shear Zone, the Mandirituba-Piraquara Shear Zone, and the Piên Shear Zone, or from granites that intruded and released fluids (external source), like the ones mentioned earlier. According to Weinberg and Hasalová (2015), shear zone movement can attract regional fluids due to the creation of pressure gradients. Sawyer (2008) divided the fluid movement during migmatization into three stages. The first is on the order of millimeter to centimeter; the second on the order of centimeter to meter; and the third on the order of tens to hundreds of meters (migmatite/granite boundary). The Atuba Complex can be classified as the second stage of melt mobility in the first migmatization phase and the third stage in the second phase.

Foliations

This section of the article proposes an in-depth analysis of the S_{n-1} and S_n foliations, crucial elements in understanding the tectonic evolution of the Atuba Complex. The foliations, characterized by planes of alignment, orientation, and mineral stretching, offer evidence of the geological events that affected the region.

S_{n-1}

The S_{n-1} foliation occurs in migmatites of the first migmatization phase and felsic granulites, with granulite facies metamorphism and ages between 2100 Ma and 2400 Ma (Siga Junior *et al.* 2007). Probably the S_{n-1} foliation is the same age as granulite facies metamorphism. The surface has a NW-SE direction and a low to high dip angle toward NE or SW. The mean attitude is N45W/55NE, with N135/35 and N40/40 lineations. The stretching lineation, folding, and foliation may suggest a thrust deformation phase, and the high angle of the planes was possibly generated from the generalized deformation of the later transcurrent-transpressive phase. Salamuni (1998) and Gonçalves (2012) also observed the S_{n-1} foliation in the Atuba Complex as a surface transposed by the S_n foliation.

The Paleoproterozoic gneisses of the Registro Complex are aged between 1.9 Ga and 2.2 Ga, with associated granulite facies metamorphism (Passarelli 2001). They may exhibit a gneissic foliation record with a NW-SE direction, probably related to the S_{n-1} foliation of the present work.

S_n

The S_n foliation is related to the second-phase migmatites and associated rocks and was interpreted as generated in a transcurrent-transpressive regime. It shows a NE-SW direction, with moderate to high dips toward SE or NW. The maximum plane is equivalent to N47W/83NW, with mineral stretching lineation N35/35, N50/5, N110/30, N240/10, and N325/70. The linear structures were defined by the orientation of biotite or the stretching of quartz and feldspars. Kinematic indicators suggest that the movement was left-lateral. The S_n surface was

interpreted as generated in a transcurrent-transpressive regime associated with the Lancinha Transcurrent System (STL), which was defined by Fiori *et al.* (1987). The Curitiba Shear Zone and the Lancinha Shear Zone are in the northernmost portion of the working area and corroborate this perspective.

Transpressional, progressive, and partitioned deformation was suggested by Ebert and Hasui (1998) for the Ribeira Belt; by Dehler *et al.* (2007) in the Serra do Azeite Shear Zone; by Faleiros *et al.* (2016) in four deformation phases (D3-D6) of the southern Ribeira Belt; by Fossen *et al.* (2019) for the entire Ribeira Belt; by Ribeiro *et al.* (2019) along the Taxaquara Shear Zone; by Baldin *et al.* (2020a, 2020b) in the Atuba Complex; and by Conte *et al.* (2020) in the Lancinha Shear Zone. The rocks noted in this deformation phase may have ages between 620 and 600 Ma (Siga Junior *et al.* 2007). These ideas correlate with Silva (2005), who depicts the Atuba Complex with Neoproterozoic leucosomes.

The Registro Complex can be correlated to the Atuba Complex (Passarelli 2001), as it features Neoproterozoic metatexites and diatexites with agmatitic, phlebitic, surreitic, schlieren, schollen, and folded structures, as well as a variety of granitoids (Passarelli *et al.* 2018), which are like the rocks observed in the Atuba Complex. The mylonitic foliation shows a NE-SW and E-W direction, with a moderate to high dip toward the N-NW, parallel to the Itariri and Cubatão shear zones (Passarelli *et al.* 2018), pointing to some relationship with the S_n foliation of the current study.

Conte *et al.* (2020) studied the Lancinha Shear Zone and associated zones and found recrystallized quartz grains by bulging, subgrain rotation or GBM, flattening, ribbons, plagioclase grains with deformation twinning, anastomosed foliations, pressure shadows, biotite fish, S-C fabric, and kinematic indicators with left-lateral movement. The left-lateral movement of the Lancinha Shear Zone is compatible with the Purunã and Serra do Azeite shear zones movement directions (Faleiros *et al.* 2011, 2016). The three zones strike in the NE-SW direction and are parallel to and subparallel to each other. All the features observed in the study by Conte *et al.* (2020) corroborate the S_n foliation of the current work.

Relationship of migmatite structures in the tectonic history of the Atuba Complex

The integrated analysis of geology, petrography, and structural geology of the Atuba Complex allowed a deep interpretation of the characteristics of the migmatites present in the region, revealing a rich geological evolution. Several types of macro- and microscopic structures were identified, and the understanding of the meaning of these structures is fundamental for the reconstruction of the tectonic history of the Atuba Complex and its relations with the Curitiba Terrane and the Ribeira Belt.

The structures of the migmatites of the Atuba Complex are indicative of intense tectonic processes that occurred during its geological evolution. Patch, schollen, folded, and stromatic structures are common in high-strain zones on a regional scale, indicating intense shear and deformation reactions in the rock. Schollen-type (rafts) migmatites may be related to paleosome fragments, refractory lithologies, or melanosomes.

The presence of xenoliths in migmatites can also be explained by the complex interaction between igneous and metamorphic processes during the geological evolution of these rocks. Xenoliths may be fragments of rock incorporated into magma during its ascension and subsequent inclusion in the resulting rocks, such as migmatites. These xenoliths may have resisted complete melting due to specific thermal and compositional conditions. In areas of contact zones between intrusive igneous bodies and host rocks, there may be xenoliths, contributing to the hybrid composition of migmatites. Another hypothesis may be related to the metamorphic processes associated with the formation of migmatites. Metamorphic temperature and pressure conditions resulting from granulite facies can cause partial melting of pre-existing metamorphic rocks. Fragments of these rocks can be incorporated into partially molten magma, forming xenoliths. Furthermore, metamorphic fluids can transport xenoliths from adjacent rocks to the region where partial melting occurs. These xenoliths can then be incorporated into the migmatite. These structures suggest the occurrence of metamorphic conditions of high temperature and pressure, possibly related to tectonic events of collision or convergence of plates, generating folding and accommodating large deformations, probably associated with large-scale tectonic events.

The schlieric, dilation-structured, and net-structured structures indicate the existence of more complex deformation zones, probably associated with lateral movements along faults or shear zones. These structures suggest that the Atuba Complex may have been affected by strike-slip tectonic regimes over geological time. The protomylonitic, ultramylonitic, and ophiolitic structures observed in the Atuba Complex migmatites are characteristics of intense ductile deformation. These structures are also indicative of processes related to shear zones, possibly associated with strike-slip regimes.

The venulated structures are suggestive of later tectonic processes that affected the Atuba Complex migmatites. These structures may be the result of distensive tectonic events on a smaller scale, associated with fracture and shear zones, indicating the occurrence of tectonic events at the end or after the ductile deformation.

The observed macrostructures and microstructures, such as folds, faults, and shear zones, are related to large-scale tectonic processes, in addition to complex metamorphic processes and intense deformation, which affected the Atuba Complex region. These structures can be the result of tectonic movements, such as the collision of plates and strike-slip.

In short, the interpretation of the characteristics described in the migmatites of the Atuba Complex allows us to reconstruct the complex tectonic history of this region. The different structures observed indicate a multifaceted tectonic evolution, with deformation and metamorphism events that occurred over geological time. This information is crucial for a more complete understanding of the geological evolution of the Atuba Complex, as well as the Curitiba Terrane and the Ribeira Belt, and contributes to a significant advance in the geological knowledge of this key area of Brazil. We hope this study will stimulate future research and contribute to the continued development of geological studies in the region and beyond.

Brittle structures

The faults and joints found in the area reflect overlapping tectonic episodes. There are brittle or brittle-ductile structures impressed in the Atuba Complex striking NE-SW direction and NW-SE lineaments associated with the Ponta Grossa Arch, represented by basic dikes, fractures, and distension faults, transversal to the basement structures (Salamuni 1998). According to Ferreira (1982), the Ponta Grossa Arch is relevantly located between the São Jerônimo-Curiúva and Rio Alonzo Lineaments, where this research was carried out. In the Curitiba region, these structures cut through Serra do Mar granites and Atuba Complex migmatites. The faults show general directions between N40° and 70°W (Putzer 1953). The fractures observed in the study area have various lengths and promote grain size reduction. At the microscale, fracturing is the main deformation mechanism, but it is accompanied by plastic deformation features. Microstructural features in feldspar crystals and quartz grains point out that the cataclases of the Atuba Complex were deformed at temperatures below 300°C (Fossen and Cavalcante 2017). Microkinks occur as isolated structures in quartz and are probably associated with cataclastic aspects at dislocation tangle sites (Tullis and Yund 1987) and suggest dislocation glide (Passchier and Trouw 2005).

The transcurrent shear zones located in the southern and southeastern Brazilian portions developed from the collision of crustal masses that led to the formation of Western Gondwana during the Ediacaran-Cambrian transition because of the consolidation of the Kalahari, Paranapanema, Rio de la Plata, and São Francisco cratons, combining the lateral-escape tectonics with a vertical component because of an oblique movement between the blocks. The transpressional character is characterized in the Southern Ribeira Belt by the Lancinha Shear Zone and in the Dom Feliciano Belt by the Major Gercino-Sierra Ballena Shear Zone (Passarelli *et al.* 2011).

The paleostress study based on the method of Angelier and Mechler (1977) allowed the finding of a NE-SW sigma 1 associated with a NW-SE sigma 3 for the left-lateral faults and an E-W sigma 1 related to an N-S sigma 3 for the right-lateral faults. The data allow us to highlight an N43E (left-lateral) and an N86W or E-W (right-lateral) main compression. From the field data, it was possible to suggest a superimposition of the right-lateral transcurrent faults over the left-lateral transcurrent faults. These data corroborate the work of Passarelli *et al.* (2004), where an N20E-N40E main compression was responsible for the left-lateral movement of the Itariri Shear Zone during the juxtaposition of the Embu and Curitiba/Registro terranes in a period between 620 Ma and 600 Ma. In the Sierra Ballena Shear Zone, the compressional component with an NE-SW orientation is also recorded and associated with movements before the main phase (Oyhantçabal *et al.* 2009). General compression between E-W and N65W is observed in virtually the entire Ribeira Belt (Passarelli *et al.* 2011) and supports the right-lateral strike-slip faulting results found in the Atuba Complex. Similarly, Ebert and Hasui (1998) observed that the Ribeira Belt underwent right-lateral transpression generated by an oblique collision in the E-W direction. Probably the sigma 1 (NE-SW) linked to a sigma

3 (NW-SE) of the left-lateral movement is also related to the ductile deformation of the rocks of the Atuba Complex since an S_n foliation in the NE-SW direction was found in the study area with left-lateral kinematics. We suggest that this sigma 1 (NE-SW) developed asymmetric and left-lateral features in the S_n foliation (D_n deformation phase) and later faults with left-lateral movement, acting in the generation of ductile and brittle features. Left-lateral faults were later superimposed by right-lateral faults with sigma 1 approximately E-W and sigma 3 N-S. The difference in stress fields for the Atuba Complex may have occurred in the Neoproterozoic, around 600 Ma (Siga Junior *et al.* 2007), and be related to local variations due to heterogeneities in the crust.

The high-grade metamorphism of the Paulo Leminski quarry was dated by the U-Pb method around 2100 ± 10 Ma (Basei *et al.* 1999). The gabbro dike observed in this quarry may be correlated with the calymmian gabbro-dioritic dikes intruding the Riacian (2100 Ma) gneisses of the Registro Complex. This is characterized southward of the Cubatão and Itariri shear zones (Passarelli 2001, Passarelli *et al.* 2004). The Calymmian extensional event was recorded by U-Pb SHRIMP (zircon) dating at 1430 Ma (Passarelli *et al.* 2012), finding that during the Mesoproterozoic there was some activity in the Curitiba Terrane.

CONCLUSION

The study area consists mainly of migmatites from the Atuba Complex, established in the Curitiba Terrane domain and located mainly in the city of Curitiba and surrounding regions. The migmatites found in the first migmatization phase are called patch, stromatic, schollen, and folded-structured. Secondarily banded or massive felsic granulites occur. The migmatites of the second migmatization phase exhibit dilation, net, stromatic, protomylonitic to ultramylonitic, schollen, schlieric, folded, ophthalmitic, and venulated structures. The rocks associated with the Atuba Complex observed in the area studied are amphibolites, granitoids, quartzites, schists, phyllites, and cataclasites, besides diabase and lamprophyre dikes, pseudotachylites, and veins that cut the lithologies.

The Atuba Complex presents two distinct types of planar and ductile linear elements; they are:

- structures (D_{n-1}) with the generation of compositional banding (S_{n-1}) from low to high dip angles to SW or NE. The paragenesis indicates granulite facies. In this context, the first phase of migmatization occurs, generating granodioritic-tonalitic leucosomes and melanosomes formed by mafic minerals (diopside, garnet, and enstatite);
- structures (D_n) constituted by mylonitic foliation (S_n) in the NE-SW direction and a low to high dip angle to the SE or NW. Metamorphic facies correspond to medium- to high-grade (amphibolite to granulite). At this juncture, the second phase of migmatization occurs, forming granitic leucosomes.

According to the analysis of microstructural features, it was possible to observe that the deformation occurred mainly

by dislocation creep mechanisms associated with dynamic recrystallization processes.

A late episode of the Atuba Complex is retrometamorphism, generating mineral alteration and quartz recrystallization by bulging at greenschist facies temperatures. Hydrothermalism (post-metamorphic stage) can be observed in the generation of sericitization, chloritization, epidotization, and carbonation in some rocks.

ACKNOWLEDGMENTS

The authors thank the Coordination of Improvement of Higher Education Personnel (CAPES), the Universidade Federal do Paraná (UFPR), the UFPR Geology Graduate Program, and the Laboratory of Mineral and Rock Analysis (LAMIR), which, through their support, contributed to the development of this research. The authors also thank Dr. Eduardo Chemas Hindi, Dr. Dina Isabel Guerreiro Cabrita for granting photographs and photomicrographs, and Dr. Frederico Meira Faleiros for the discussions on petrography. Furthermore, the authors would like to thank the reviewers who dedicated their time to improving the quality of the manuscript.

ARTICLE INFORMATION

Manuscript ID: 20230016. Received on: 25 APR. 2023. Approved on: 23 JAN 2024.

How to cite: Baldin M.T., Salamuni E., Lagoeiro L.E., Sanches E. (2023). Advancing geological and structural understanding of the Atuba Complex: a study in the Curitiba Terrane of the Southern Ribeira Belt, Southern Brazil. *Brazilian Journal of Geology*, 54(1), e20230016. <https://doi.org/10.1590/2317-4889202420230016>

M.T.B.: Conceptualization, Data curation, Formal analysis, Investigation, Methodology, Validation, Visualization, Writing – original draft, Writing – review & editing; E.S.: Conceptualization, Funding acquisition, Project administration, Resources, Supervision; L.E.L.: Funding acquisition, Resources, Supervision; E.S.: Visualization, Writing – review & editing.

REFERENCES

- Almeida F.F.M., Amaral G., Cordani U.G., Kawashita K. 1973. The Precambrian evolution of the South America Cratonic Margin South of the Amazon River. In: Nairn E.M., Stehli F.G. (eds.). *The Ocean basins and margins*. New York: Plenum Publishing Corporation, v. 1, p. 411-446. https://doi.org/10.1007/978-1-4684-3030-1_11
- Angelier J., Mechler P. 1977. Sur une méthode graphique de recherche des contraintes principales également utilisable en tectonique et en séismologie: la méthode des dièdres droits. *Bulletin de la Société Géologique de France*, 7(6):1309-1318. <https://doi.org/10.2113/gssgfbull.S7-XIX.6.1309>
- Ashworth J.R. 1985. *Migmatites*. Glasgow: Blackie, 302 p.
- Baldin M.T., Salamuni E., Lagoeiro L.E. 2020a. Quantificação da deformação em metatexitos estromáticos e rochas associadas do Complexo Atuba, Cinturão Ribeira Meridional. *Geociências (UNESP)*, 39(3):631-660. <https://doi.org/10.5016/geociencias.v39i03.14391>
- Baldin M.T., Salamuni E., Lagoeiro L.E. 2020b. Petrographic, structural and textural analysis of the Atuba Complex, Southern Ribeira Belt: Case study

- in the Greca quarry. *Journal of South American Earth Sciences*, **104**, 102821. <https://doi.org/10.1016/j.jsames.2020.102821>
- Basei M.A.S., Frimmel H.E., Nuttman A.P., Preciozzi F. 2008. West Gondwana amalgamation based on detrital zircon ages from Neoproterozoic Ribeira and Dom Feliciano belts of South America and comparison with coeval sequences from SW Africa. In: Pankhurst R.J., Trow R.A.J., Brito Neves B.B., Witt, D. (eds.). *West Gondwana: Pre-Cenozoic Correlations Across the South Atlantic Region*. London: Geological Society, Special Publication, v. 294, p. 239-256. <https://doi.org/10.1144/SP294.13>
- Basei M.A.S., Nutman A., Siga Junior O., Passarelli C.R., Drukas C.O. 2009. The evolution and tectonic setting of the Luis Alves microplate of southeastern Brazil: an exotic terrane during the assembly of western Gondwana. *Developments in Precambrian Geology*, **16**:273-291. [https://doi.org/10.1016/S0166-2635\(09\)01620-X](https://doi.org/10.1016/S0166-2635(09)01620-X)
- Basei M.A.S., Siga Junior O., Machiavelli A., Mancini F. 1992. Evolução tectônica dos terrenos entre os Cinturões Ribeira e Dom Feliciano (PR - SC). *Revista Brasileira de Geociências*, **22**(2):216-221. <https://doi.org/10.25249/0375-7536.1992216221>
- Basei M.A.S., Siga Junior O., Reis Neto J.M., Passarelli C.R., Prazeres H.J., Kaulfuss G., Sato K., Lima P.S. 1999. Paleoproterozoic granulitic Belts of the Brazilian Southern Region (PR-SC). *LL South American Symposium on Lsotope Geology*. p. 291-294.
- Bigarella J.J., Salamuni R. 1956. Estudos preliminares na Série Açungui VII: algumas estruturas sinênticas nos dolomitos da Formação Capiru. *Arquivos de Biologia e Tecnologia*, **11**:197-205.
- Brito Neves B.B., Cordani U.G. 1991. Tectonic evolution of South America during Late Proterozoic. *Precambrian Research*, **53**(1-2):23-40. [https://doi.org/10.1016/0301-9268\(91\)90004-T](https://doi.org/10.1016/0301-9268(91)90004-T)
- Brown M. 1973. The definition of metatexis, diatexis and migmatite. *Proceedings of the Geologists' Association*, **84**(Part 4):371-382. [https://doi.org/10.1016/S0016-7878\(73\)80021-5](https://doi.org/10.1016/S0016-7878(73)80021-5)
- Brown M. 1979. The petrogenesis of the St-Malo migmatite belt, Armorican Massif, France, with particular reference to the diatexites. *Neues Jahrbuch für Mineralogie*, **135**:48-74.
- Brown M. 1994. The generation, segregation, ascent and emplacement of granite magma: the migmatite-to-crustally-derived granite connection in thickened orogens. *Earth-Science Reviews*, **36**(1-2):83-130. [https://doi.org/10.1016/0012-8252\(94\)90009-4](https://doi.org/10.1016/0012-8252(94)90009-4)
- Brown M. 1998. Unpairing metamorphic belts: P-T paths and a tectonic model for the Ryoke Belt, southwest Japan. *Journal of Metamorphic Geology*, **16**(1):3-22. <https://doi.org/10.1111/j.1525-1314.1998.00061.x>
- Brown M. 2013. Granite: From genesis to emplacement. *Bulletin of the Geological Society of America*, **125**(7-8):1079-1113. <https://doi.org/10.1130/B30877.1>
- Bucher K., Grapes R. 2011. *Petrogenesis Of Metamorphic Rocks*. 8. ed. Springer, 428 p.
- Cabrita D.I.G. 2015. *Análise da deformação em tectonitos do bloco sul da Zona de Cisalhamento Curitiba (PR)*. Dissertação de Mestrado, Departamento de Geologia, Universidade Federal do Paraná, Curitiba, 92 p.
- Campagnoli F. 1996. *Considerações sobre a geologia da Sequência Turvo-Cajati, na região do Alto Rio Jacupiranguinha, SP*. Dissertação de Mestrado, Universidade de São Paulo, São Paulo, 96 p.
- Campanha G.A.C., Brito Neves B.B. 2004. Frontal and oblique tectonics in the Brazilian Shield. *Episodes*, **27**(4):255-259. <https://doi.org/10.18814/epiugs/2004/v27i4/003>
- Campanha G.A.C., Sadowski G.R. 1999. Tectonics of the Southern Portion of the Ribeira Belt (Apliaí Domain). *Precambrian Research*, **98**(1-2):31-51. [https://doi.org/10.1016/S0301-9268\(99\)00027-3](https://doi.org/10.1016/S0301-9268(99)00027-3)
- Conte T., Cavalcante C., Lagoeiro L.E., Fossen H., Silveira C.S. 2020. Quartz textural analysis from an anastomosing shear zone system: Implications for the tectonic evolution of the Ribeira belt, Brazil. *Journal of South American Earth Sciences*, **103**, 102750. <https://doi.org/10.1016/j.jsames.2020.102750>
- Cury L.F. 2009. *Geologia do terreno Paranaguá*. Tese de Doutorado, Instituto de Geociências, Universidade de São Paulo, São Paulo, 202 p. <https://doi.org/10.11606/T.44.2009.tde-06072009-113335>
- Dehler N.M., Machado R., Fassbinder E. 2007. Shear structures in the Serra do Azeite shear zone, southeastern Brazil: transtensional deformation during regional transpression in the central Mantiqueira province (Ribeira belt). *Journal of South American Earth Sciences*, **23**(2-3):176-192. <https://doi.org/10.1016/j.jsames.2006.09.017>
- Delvaux D., Sperner B. 2003. Stress tensor inversion from fault kinematic indicators and focal mechanism data: the TENSOR program. In: Nieuwland D. (Ed.). *New insights into structural interpretation and modelling*. London: Geological Society, Special Publications.
- Doblas M. 1998. Slickenside kinematic indicators. *Tectonophysics*, **295**(1-2):187-197. [https://doi.org/10.1016/S0040-1951\(98\)00120-6](https://doi.org/10.1016/S0040-1951(98)00120-6)
- Ebert H.D., Hasui Y. 1998. Transpressional tectonics and strain partitioning during oblique collision between three plates in the Precambrian of southeast Brazil. In: Holdsworth R.E., Strachan R.A., Dewey J.F. (eds.). *Continental Transpressional and Transtensional Tectonic*. London: Geological Society, Special Publications. v. 135, p. 231-252.
- Faleiros F.M. 2008. *Evolução de terrenos tectono-metamórficos da serra da Ribeira e Planalto Alto Turvo (SP, PR)*. Tese de doutorado, Instituto de Geociências, Universidade de São Paulo, São Paulo, 318 p. <https://doi.org/10.11606/T.44.2008.tde-02092008-113513>
- Faleiros F.M., Campanha G.A.C., Martins L., Vlach S.R.F., Vasconcelos P.M. 2011. Ediacaran high-pressure collision metamorphism and tectonics of the southern Ribeira Belt (SE Brazil): Evidence for terrane accretion and dispersion during Gondwana assembly. *Precambrian Research*, **189**(3-4):263-291. <https://doi.org/10.1016/j.precamres.2011.07.013>
- Faleiros F.M., Campanha G.A.C., Pavan M., Almeida V.V., Rodrigues S.W.O., Araujo B.P. 2016. Short-lived polyphase deformation during crustal thickening and exhumation of a collisional orogen (Ribeira Belt, Brazil). *Journal of Structural Geology*, **93**:106-130. <https://doi.org/10.1016/j.jsg.2016.10.006>
- Ferreira F.J.F. 1982. *Integração de Dados Aeromagnéticos e Geológicos: Configuração e Evolução Tectônica do Arco de Ponta Grossa*. Dissertação de Mestrado, Instituto de Geociências, Universidade de São Paulo, São Paulo, 186 p. <https://doi.org/10.11606/D.44.1983.tde-14082013-161535>
- Fiori A.P., Fassbinder E., Gois J.R., Fumagalli C.E. 1987. Compartimentação tectônica do Grupo Açungui a norte de Curitiba. *III Simpósio Sul-Brasileiro de Geologia*. Atas, 1, 183-196.
- Forero-Ortega A.J., Campanha G.A.C., Faleiros F.M. 2020. Pure shear-dominated transpression and vertical extrusion in a strike-slip fault splay from the Itapirapuã Shear Zone, Ribeira Belt, Brazil. *Tectonophysics*, **786**, 228455. <https://doi.org/10.1016/j.tecto.2020.228455>
- Fossen H., Cavalcante G.C.G. 2017. Shear zones – A review. *Earth-Science Reviews*, **171**:434-455. <https://doi.org/10.1016/j.earscirev.2017.05.002>
- Fossen H., Cavalcante G.C.G., Pinheiro R.V.L., Archanjo C.J. 2019. Deformation – Progressive or multiphase? *Journal of Structural Geology*, **125**:82-99. <https://doi.org/10.1016/j.jsg.2018.05.006>
- Fronza G., Gilveira C.T., Fiori A.P., Salamuni E., Nascimento E.R., D'aroz P., Mottin T.E. 2016. Aplicativos para geração de estereogramas e classificação de rochas ígneas. *Congresso Brasileiro de Geologia*. Anais, SBG, 48, 1.
- Fuck R.A., Trein E., Marini O.J. 1967. Geologia e petrografia dos migmatitos do Paraná. *Boletim Paranaense de Geociências*, **23-25**:5-41.
- Gardien V., Thompson A.B., Ulmer P. 2000. Melting of biotite + plagioclase + quartz gneisses; the role of H₂O in the stability of amphibole. *Journal of Petrology*, **41**(5):651-666. <https://doi.org/10.1093/ptrology/41.5.651>
- Gibbon D.L., Wyllie P.J. 1969. Experimental studies of igneous rock series: the Farrington Complex, North Carolina, and the Star Mountain Rhyolite, Texas. *Journal of Geology*, **77**(2):221-239. <https://doi.org/10.1086/627423>
- Gonçalves F.M. 2012. *Caracterização da Zona de Cisalhamento Curitiba - (PR)*. Dissertação de mestrado, Departamento de Geologia, Universidade Federal do Paraná, Curitiba, 123 p.
- Heilbron M., Pedrosa-Soares A.C., Campos Neto M.C., Silva L.C., Trouw R.A.J., Janasi V.A. 2004. Província Mantiqueira. In: Mantessoneto V. et al. (eds.). *Geologia do Continente Sul-Americano: evolução da obra de Fernando Flávio Marques de Almeida*. São Paulo, Beca, p. 203-234.
- Heilbron M., Valeriano C.M., Tassinari C.C.G., Almeida J.C.H., Tupinambá M., Siga Junior O., Trouw R.A.J. 2008. Correlation of Neoproterozoic terranes between the Ribeira Belt, SE Brazil and its African counterpart: comparative

- tectonic evolution and open questions. In: Pankhurst R.J., Trouw R.A.J., Brito Neves B.B., De Wit M. (Eds.). *West Gondwana Pre-cenozoic Correlations across the South Atlantic Region*. London: Geological Society London, v. 294, p. 211-232.
- Holland T., Blundy J. 1994. Non-ideal interactions in calcic amphiboles and their bearing on amphibole-plagioclase thermometry. *Contributions to Mineralogy and Petrology*, **116**:433-447. <https://doi.org/10.1007/BF00310910>
- Jin Z., Green H.W., Zhou Y. 1994. Melt topology in partially molten mantle peridotite during ductile deformation. *Nature*, **372**:164-167. <https://doi.org/10.1038/372164a0>
- Johnston A.D., Wyllie P.J. 1988. Interaction of granitic and basic magmas: experimental observations on contamination processes at 10 kbar with H₂O. *Contributions to Mineralogy and Petrology*, **98**:352-362. <https://doi.org/10.1007/BF00375185>
- Jurewicz S.R., Watson E.B. 1984. Distribution of partial melt in a felsic system: the importance of surface energy. *Contributions to Mineralogy and Petrology*, **85**:25-29. <https://doi.org/10.1007/BF00380218>
- Kaulfuss G.A. 2001. *Geocronologia dos Núcleos de Embasamento Setuva, Betara e Tigre, Norte de Curitiba-PR*. Dissertação de Mestrado, Instituto de Geociências, Universidade de São Paulo, São Paulo, 115 p. <https://doi.org/10.11606/D.44.2001.tde-25092015-162857>
- Kruhl J.H. 1996. Prism and basal plane parallel subgrain boundaries in quartz: a microstructural geothermobarometer. *Journal of Metamorphic Geology*, **14**(5):581-589. <https://doi.org/10.1046/j.1525-1314.1996.00413.x>
- Machado R., Dehler N.M., Vasconcelos P. 2007. ⁴⁰Ar/³⁹Ar ages (600-570 Ma) of the Serra do Azeite transtensional shear zone: evidence for syncontractional extension in the Cajati area, southern Ribeira belt. *Anais da Academia Brasileira de Ciências*, **79**(4):713-723. <https://doi.org/10.1590/S0001-37652007000400011>
- Mainprice D., Bouchez J.L., Blumenfeld P., Tubia J.M. 1986. Dominant c slip in naturally deformed quartz: implications for dramatic plastic softening at high temperature. *Geology*, **14**(10):819-822. [https://doi.org/10.1130/0091-7613\(1986\)14<819:DCSIND>2.0.CO;2](https://doi.org/10.1130/0091-7613(1986)14<819:DCSIND>2.0.CO;2)
- Marchildon N., Brown M. 2003. Spatial distribution of melt-bearing structures in anatectic rocks from southern Brittany, France: implications for melt transfer at grain-to orogen-scale. *Tectonophysics*, **364**:215-235.
- Mehnert K.R. 1968. *Migmatites and the origin of granitic rocks*. Amsterdam: Elsevier, 405 p.
- Mineropar. 2006a. *Folha de Curitiba (SG.22-X-D)*. Curitiba, escala 1:250.000. Available at: <http://www.mineropar.pr.gov.br>. Accessed on: Sept. 10, 2020.
- Mineropar. 2006b. *Folha de Ponta Grossa (SG.22-X-C-II)*. Curitiba, escala 1:250.000. Available at: <http://www.mineropar.pr.gov.br>. Accessed on: Sept. 10, 2020.
- Olsen S.N., Grant J.A. 1991. Isocon analysis of migmatization in the Front Range, Colorado, USA. *Journal of Metamorphic Geology*, **9**(2):151-164. <https://doi.org/10.1111/j.1525-1314.1991.tb00511.x>
- Oyhantçabal P., Siegesmund S., Wemmer K., Layer P. 2009. The Sierra Ballena Shear Zone in the southernmost Dom Feliciano Belt (Uruguay): evolution, kinematics, and deformation conditions. *International Journal of Earth Sciences (Geologische Rundschau)*, **99**:1227-1246. <https://doi.org/10.1007/s00531-009-0453-1>
- Passarelli C.R. 2001. *Caracterização estrutural e geocronológica dos domínios tectônicos da porção sul-oriental do Estado de São Paulo*. Tese de Doutorado, Instituto de Geociências, Universidade de São Paulo, São Paulo, 254 p. <https://doi.org/10.11606/T.44.2001.tde-03022014-155518>
- Passarelli C.R., Basei M.A.S., Prazeres Filho H.J., Siga Junior O. 2004. The Cubatão-Itariri Shear System and the Serrinha Shear Zone: the limits of the Pre-Cambrian Terranes, southeastern São Paulo State-Brazil. *International Geological Congress*, 32.
- Passarelli C.R., Basei M.A.S., Prazeres Filho H.J., Siga Junior O. 2012. First evidence of Calimian basic magmatism in Registro Terrane-Ribeira Belt-State of São Paulo. *VIII South American Symposium on Isotope Geology*, Medellin, 53.
- Passarelli C.R., Basei M.A.S., Siga Junior O., Harara O.M.M. 2018. The Luís Alves and Curitiba Terranes: Continental Fragments in the Adamastor Ocean. In: Siegesmund S., Basei M., Oyhantçabal P., Oriolo S. (eds.). *Geology of Southwest Gondwana*. Cham: Springer, p. 189-216. https://doi.org/10.1007/978-3-319-68920-3_8
- Passarelli C.R., Basei M.A.S., Wemmer K., Siga Junior O., Oyhantçabal P. 2011. Major shear zones of southern Brazil and Uruguay: escape tectonics in the eastern border of Rio de la Plata and Paranapanema cratons during the Western Gondwana amalgamation. *International Journal of Earth Sciences (Geologische Rundschau)*, **100**:391-414. <https://doi.org/10.1007/s00531-010-0594-2>
- Passchier C.W., Trouw R.A.J. 2005. *Microtectonics*. Berlin: Springer-Verlag, 289 p.
- Paterson S.R., Vernon R.H., Tobisch O.T. 1989. A review of criteria for the identification of magmatic and tectonic foliations in granitoids. *Journal of Structural Geology*, **11**(3):349-363. [https://doi.org/10.1016/0191-8141\(89\)90074-6](https://doi.org/10.1016/0191-8141(89)90074-6)
- Patiño Douce A.E. 1996. Effects of pressure and H₂O content on the compositions of primary crustal melts. *Earth Sciences*, **87**(1-2):11-21. <https://doi.org/10.1017/S026359330000643X>
- Petit J.P. 1987. Criteria for sense of movement on fault surfaces in brittle rocks. *Journal of Structural Geology*, **9**(5-6):597-608. [https://doi.org/10.1016/0191-8141\(87\)90145-3](https://doi.org/10.1016/0191-8141(87)90145-3)
- Putzer H. 1953. Diastrofismo "Germanótipo" e suas relações com o vulcanismo basáltico na parte meridional de Santa Catarina. *Boletim da Sociedade Brasileira de Geologia*, **2**(1):37-71.
- Ribeiro T.B.V., Faleiros F.M., Campanha G.A.C., Lagoeiro L., Weinberg R.F., Hunte N.J.R. 2019. Kinematics, nature of deformation and tectonic setting of the Taxaquara Shear Zone, a major transpressional zone of the Ribeira Belt (SE Brazil). *Tectonophysics*, **751**:83-108. <https://doi.org/10.1016/j.tecto.2018.12.025>
- Ricardo B.S., Faleiros F.M., Moraes R., Siga Junior O., Campanha G.A.C. 2020. Tectonic implications of juxtaposed high- and low-pressure metamorphic field gradient rocks in the Turvo-Cajati Formation, Curitiba Terrane, Ribeira Belt, Brazil. *Precambrian Research*, **345**:105766. <https://doi.org/10.1016/j.precamres.2020.105766>
- Salamuni E. 1998. *Tectônica da Bacia Sedimentar de Curitiba (PR)*. Tese de Doutorado, Instituto de Geociências e Ciências Exatas, Universidade Estadual Paulista, Rio Claro, 214 p.
- Santos L.R., Cury L.F., Rosenblume J., Mendes M.T., Fedalto G., Lopes A.P., Leandro R., Siga Junior O., Basei M. 2022. Tracing the continental margins of the Southern Ribeira belt, Brazil: Provenance and connections of post-Rodinia fragments. *Precambrian Research*, **378**:106756. <https://doi.org/10.1016/j.precamres.2022.106756>
- Santos L.R., Spisila A.L., Guimarães D.P., Szameit L., Bongioiolo A.B.S., Cury L.F. 2021. The geology of the Capiru Group, Curitiba Terrane, Southern Ribeira Belt (Brazil). *Journal of Maps*, **17**(2):638-646. <https://doi.org/10.1080/17445647.2021.1982036>
- Sato K., Siga Junior O., Nutman A.P., Basei M.A.S., McCreath I., Kaulfuss G. 2003. The Atuba Complex, Southern South American Platform: Archean Components and Paleoproterozoic to Neoproterozoic Tectonothermal Events. *Gondwana Research*, **6**(2):251-263. [https://doi.org/10.1016/S1342-937X\(05\)70974-6](https://doi.org/10.1016/S1342-937X(05)70974-6)
- Sato K., Siga Junior O., Silva J.A., McCreath I., Duny L., Lizuka T., Rino S., Hirata T., Sproesser W., Basei M.A.S. 2009. In situ Isotopic Analyses of U and Pb in Zircon by Remotely Operated SHRIMP II, and Hf by LA-ICP-MS: an Example of Dating and Genetic Evolution of Zircon by ¹⁷⁶Hf/¹⁷⁷Hf from the Ita Quarry in the Atuba Complex, SE Brazil. *Geologia USP. Série Científica*, **9**(3):61-69. <https://doi.org/10.5327/z1519-874x2009000300004>
- Sawyer E.W. 1998. Formation and evolution of granite magmas during crustal reworking: the significance of diatexites. *Journal of Petrology*, **39**(6):1147-1167.
- Sawyer E.W. 1999. Criteria for the recognition of partial melting. *Physics and Chemistry of the Earth*, **24**(3):269-279. [https://doi.org/10.1016/S1464-1895\(99\)00029-0](https://doi.org/10.1016/S1464-1895(99)00029-0)
- Sawyer E.W. 2001. Melt segregation in the continental crust: distribution and movement of melt in anatectic rocks. *Journal of Metamorphic Geology*, **19**(3):291-309. <https://doi.org/10.1046/j.0263-4929.2000.00312.x>

- Sawyer E.W. 2008. *Atlas of migmatites*. Canada: NRC Research Press, 371 p. <https://doi.org/10.1139/9780660197876>
- Sawyer E.W., Brown M. 2008. *Working with migmatites*. Canada: Mineralogical Association of Canada, 158 p.
- Schmid S.M., Handy M.R. 1991. Towards a genetic classification of fault rocks: geological usage and tectonophysical implications. In: Moller D.W., Mckenzie J.A., Weissert H. (eds). *Controversies in Modern Geology*. Londres: Academic Press, p. 339-361.
- Sibson R.H. 1977. Fault rocks and fault mechanisms. *Journal of Geological Society of London*, **133**:191-213. <https://doi.org/10.1144/gsjgs.133.3.0191>
- Siga Junior O. 1995. *Domínios tectônicos do sudeste do Paraná e nordeste de Santa Catarina: Geocronologia e evolução crustal*. Tese de Doutorado, Instituto de Geociências, Universidade de São Paulo, São Paulo, 212 p. <https://doi.org/10.11606/T.44.1995.tde-05112013-093542>
- Siga Junior O., Basei M.A.S., Passarelli C.R., Harara O.M., Sato K., Cury L.F., Prazeres Filho H.J. 2007. Geocronologia de rochas gnáissico-migmatíticas e sienograníticas do Núcleo Setuva (PR): Implicações Tectônicas. *Revista Brasileira de Geociências*, **37**:114-128. <https://doi.org/10.25249/0375-7536.2007371114128>
- Siga Junior O., Basei M.A.S., Reis Neto J.M., Machiavelli A., Harara O.M. 1995. O Complexo Atuba: um cinturão Paleoproterozoico intensamente retrabalhado no Neoproterozoico. *Geologia USP. Série Científica*, **26**:69-98. <https://doi.org/10.11606/issn.2316-8986.v26i0p69-98>
- Silva J.A. 2005. *Petrologia e geoquímica dos gnaisses migmatíticos do Complexo Atuba, Curitiba PR*. Dissertação de Mestrado, Instituto de Geociências, Universidade de São Paulo, São Paulo, 153 p. <https://doi.org/10.11606/D.44.2005.tde-29092015-143212>
- Silva P.C.S., Yamato A.A., Vasconcelos C.S., Lopes Júnior I. 1998. *Projeto Folha de Curitiba (SG-22-X-D-I): Relatório Final*. São Paulo, 91 p.
- Stipp M., Stunitz H., Heibronner R., Schmid S.M. 2002. The eastern Tonale fault zone: "a natural laboratory" for crystal plastic deformation of quartz over a temperature range from 250 to 700°C. *Journal of Structural Geology*, **24**(12):1861-1884. [https://doi.org/10.1016/S0191-8141\(02\)00035-4](https://doi.org/10.1016/S0191-8141(02)00035-4)
- Tullis J., Yund R.A. 1987. Transition from cataclastic flow to dislocation creep of feldspar: mechanisms and microstructures. *Geology*, **15**(7):606-609. [https://doi.org/10.1130/0091-7613\(1987\)15<606:TFCFTD>2.0.CO;2](https://doi.org/10.1130/0091-7613(1987)15<606:TFCFTD>2.0.CO;2)
- Vanderhaeghe O., Teysier C. 2001. Partial melting and flow in orogens. *Tectonophysics*, **342**(3-4):451-472. [https://doi.org/10.1016/S0040-1951\(01\)00175-5](https://doi.org/10.1016/S0040-1951(01)00175-5)
- Vasconcelos C.S., Yamato A.A., Dehler N.M., Lopes Junior I. 1999. *Projeto Jacupiranga - Rio Guaraú, Estado de São Paulo*. São Paulo: Convênio CPRM/Secretaria de Energia do Governo do Estado de São Paulo.
- Vernon R.H. 2004. *A practical guide to rock microstructure*. Cambridge: Cambridge University Press, 594 p.
- Voll G. 1976. Recrystallization of quartz, biotite and feldspar from Erstfeld to the Leventina Nappe, Swiss Alps, and its geological significance. *Schweizerische Mineralogische und Petrographische Mitteilungen*, **56**:641-647. <https://doi.org/10.5169/seals-43709>
- Weinberg R.F., Hasalová P. 2015. Water-fluxed melting of the continental crust: A review. *Lithos*, **212-215**:158-188. <https://doi.org/10.1016/j.lithos.2014.08.021>
- White R.W., Powell R., Clarke G.L. 2003. Prograde metamorphic assemblage evolution during partial melting of metasedimentary rocks at low pressures: migmatites from Mt. Stafford, Central Australia. *Journal of Petrology*, **44**(11):1937-1960. <https://doi.org/10.1093/petrology/egg065>
- Whitney D.L., Evans B.W. 2010. Abbreviations for names of rock-forming minerals. *American Mineralogist*, **95**(1):185-187. <https://doi.org/10.2138/am.2010.3371>
- Wolf M.B., Wyllie P.J. 1994. Dehydration-melting of amphibolite at 10 kbar: the effects of temperature and time. *Contributions to Mineralogy and Petrology*, **115**:369-383. <https://doi.org/10.1007/BF00320972>
- Wyllie P.J., Wolf M.B. 1993. Amphibolite dehydration-melting: sorting out the solidus. *Geological Society Special Publication*, **76**:405-416. <https://doi.org/10.1144/GSL.SP.1993.076.01.20>
- Yardley B.W.D. 2004. *Introdução à petrologia metamórfica*. Brasília: Universidade de Brasília, 432 p.